M 2014

U.PORTO
FEUP FACULDADE DE ENGENHARIA
UNIVERSIDADE DO PORTO

Gellan Gum-Coated Gold Nanorods for Drug Delivery Applications

SÍLVIA CRISTINA ARAÚJO VIEIRA

DISSERTAÇÃO DE MESTRADO APRESENTADA
À FACULDADE DE ENGENHARIA DA UNIVERSIDADE DO PORTO EM
BIOENGENHARIA

- This page was intentionally left blank. -

Faculdade de Engenharia da Universidade do Porto

Instituto de Ciências Biomédicas Abel Salazar

FEUP

U.PORTO

INSTITUTO DE CIÊNCIAS BIOMÉDICAS ABEL SALAZAR
UNIVERSIDADE DO PORTO

Gellan Gum-Coated Gold Nanorods for Drug Delivery Applications

Sílvia Cristina Araújo Vieira

Master Thesis
Submitted in partial fulfilment
of the requirements for the Degree of
Master of Science in Bioengineering,
at the Faculdade de Engenharia da Universidade do Porto
and Instituto de Ciências Biomédicas Abel Salazar

Supervisor: Joaquim Miguel Oliveira, Pedro Granja, Rui L. Reis

September 2014

Abstract

Due to its unique properties, gold nanorods (AuNR) have been widely studied for diverse biomedical applications such as drug delivery, biosensing, bioimaging and photothermal therapy. However, as-prepared AuNR are known to be cytotoxic, due to the presence of the surfactant cetyl trimethylammonium bromide (CTAB). Bearing this drawback in mind, before use AuNR for biomedical purposes it is thus necessary to modify particles surface, making them more biocompatible and stable under biological conditions. Functionalization of AuNR with natural-based polymers that are biodegradable and biocompatible can be envisioned to circumvent the cytotoxicity issues, while enable the controlled release of drugs/bioactive agents. Herein, natural and biocompatible low acyl gellan gum (GG) was used for the first time to coat AuNR, previously modified with poly(acrylic acid sodium salt) (PAA) and poly(allylamine hydrochloride) (PAH). Transmission electron microscopy (TEM) images confirm the presence of a GG shell around individual particles, with an average size of 6.8 nm. GG-coated AuNR (AuNR-(PAA PAH GG)) display an increased stability in a wide range of pH and ionic strength conditions, when compared to the as-prepared and polymeric modified AuNR, as determined by UV-Vis spectroscopy. Particles biocompatibility was also analysed *in vitro* by means of performing a MTS assay, and no significant cytotoxicity was found for AuNR-(PAA PAH GG) after 14 days of incubation with both SaOS-2, a human osteoblast-like cell line, and rabbit adipose stem cells. Dark-field microscopy and TEM have shown that internalization of AuNR-(PAA PAH GG) occurs on both cell types and that particles stay aggregate inside cells, but in different intracellular structures. With the final aim of using these particles as drug delivery systems for bone tissue engineering, we attempted the encapsulation of dexamethasone onto AuNR-(PAA PAH GG). However, further work is needed to optimize the loading process and drug quantification.

- This page was intentionally left blank. -

Acknowledgments

I am deeply grateful to my thesis supervisor, Dr. J. Miguel Oliveira, for the opportunity, encouragement, inspiration and guidance during the last months.

I would also like to extend my gratitude to Professor Rui Reis, who gave me the opportunity to be part of 3B's group, and to Dr. Pedro Granja, that encouraged my decision since the beginning.

I also express my thankfulness to Stephanie Vial, for her precious guidance, support and promptness to answer my theoretical questions and practical problems. To her I owe most of the knowledge learnt during this project.

My sincere thanks also goes to all members of 3B's Research Group, for welcoming me amongst the group, for all support and help. Especially to Mariana Carvalho, for all the help on cell culture.

To Margarida, Sofia and Sónia (the perfect "bullying team") I would like to give a special "Thank you!" for all the help, support and, most of all, for the great friendship!; to Álvaro, for the patience and support during the bad and good moments (and, of course, for all the coffees); to the "lunch crew", for all the moments that we have shared;

But this work is not only a reflection of the last six months. It is also the conclusion of five years full of good memories. So, I would like to acknowledge my Professors and previous supervisors for all the transmitted knowledge. Also, I would like to express my deepest gratitude to my closest friends: Joana, Daniela, João Santos, João Coentro and José. With them I have passed the best moments of the last few years. And with them I was able to surpass the worst moments. Thank you with all of my heart! I extend my gratitude to Guilherme and Isabel, for all the continuous support and moments shared.

Last, but definitely not the least, I can only express my gratitude to my parents and sister for their unconditional support and patience (a lot of patience!) throughout this challenging stage of my life. Without them this would be definitely not possible. Pai, mãe e Bea: sim, acabei! E com um dedo no nariz!!

To all, thank you.

- This page was intentionally left blank. -

Table of Contents

Abstract ..... **i**

Acknowledgments ..... **iii**

Table of Contents ..... **v**

List of Figures ..... **vii**

List of Tables ..... **ix**

Glossary ..... **xi**

Chapter 1 ..... **1**

Introduction 1
1.1. Gold Nanoparticles 1
Gold Nanorods Synthesis 3
Gold Nanorods Cytotoxicity and Surface Modifications 4
1.2. Gellan Gum 10
1.3. Aim of the Project 14
1.4. Outline 16

Chapter 2 ..... **17**

Materials and Methods 17
2.1. Synthesis of Gold Nanorods 17
2.2. Surface Functionalization 17
2.3. Characterization of nanoparticles 18
2.3.1. Spectrophotometric analysis (Optical properties) 18
2.3.2. Surface Potential 18
2.3.3. Morphological characterization 18
2.4. Particles Stability 18
2.4.1. Ionic Strength 18
2.4.2. pH 19
2.5. Dexamethasone Incorporation 19
2.5.1. Fourier Transform Infrared Spectroscopy (FTIR) 19
2.6. *In vitro* studies 19
2.7. Statistical analysis and Software 21

Chapter 3 ..... **23**

Results 23

3.1. Synthesis and Characterization of Gold Nanorods 23
3.2. Surface Functionalization 24
3.3. Gellan Gum Coating 25
3.4. Stability Studies 27
Ionic Strength 27
pH effect 28
3.5. In vitro Studies 29
3.6. Incorporation of Dexamethasone 33

Chapter 4 37

Discussion 37

Chapter 5 42

Conclusions 43

References 45

List of Figures

Figure 1 – Typical UV-Vis spectrum of AuNR, with schematic representations of SPR in AuNR. 2

Figure 2 - Schematic representation of AuNR synthesis process. 3

Figure 3 - Common methods of AuNR surface modification: A-layer by layer; B – silica coating; C – displacement of the surfactant by thiol-terminated molecules; D – insertion of hydrophobic molecules; E – on-particle polymerization. 5

Figure 4 – Schematic representation of Zandberg's rational [56]. 7

Figure 5 - Schematic representation of Wijaya *et al*. rational. Selective releases were induced by selective melting of gold nanorods *via* ultrafast laser irradiation at the nanorods' LPB resonance peaks. When particles were submitted to an 800 nm irradiation (left), AuNR (blue) melts and release its cargo, DNA labelled by FAM (green triangles). Exposure to an 1100 nm irradiation (right) melt the nanobones (red), which selectively release DNA labelled with TMR (orange stars). Releases were efficient (50−80%) and externally tunable by laser fluence. Released oligonucleotides were still functional [60]. 8

Figure 6 - Flowchart of Elbakry *et al*. strategy for the production of layer-by-layer assembled AuNP for siRNA delivery [59]. 8

Figure 7 - Gellan gum structure. Native or high acyl gellan gum (upper image); low acyl gellan gum (image bellow) [108]. 11

Figure 8 - Schematic representation of gradual transformation of GG in aqueous solution, through different temperatures. Adapted from [64]. 12

Figure 9 - UV-Vis spectra of AuNR before (black line) and after (red line) the washing step. 23

Figure 10 – A: TEM images of AuNR with and 250 000x magnification; B: SEM images of AuNR with 200 000x magnification. 24

Figure 11 – Schematic representation of layer-by-layer approach for AuNR modification. 24

Figure 12 - A: UV-Vis spectra of AuNR, AuNR coated with PAA and AuNR-(PAA PAH); B: TEM image of AuNR-(PAA PAH) with a magnification of 250 000X. 25

Figure 13 – Schematic representation of AuNR-(PAA PAH) modification with GG. 25

Figure 14 – A: UV-Vis spectra of AuNR-(PAA PAH) (red line) and AuNR-(PAA PAH GG) (black line); B: UV-Vis spectra of AuNR-(PAA PAH GG) (black line) comparing to the spectrum of a 0.25% w/v GG solution (red line)..... 26

Figure 15 – A: TEM image of AUNR-(PAA PAH GG) particles with 150 000X magnification; B: TEM image of AuNR-(PAA PAH GG) with 250 000X magnification; C: SEM image of AuNR-(PAA PAH GG); D: Backscatter electron analysis of AuNR-(PAA PAH GG)..... 26

Figure 16 – UV-Vis spectrometry analysis of ionic strength influence on particles stability. Defined concentrations of NaCl were added to solutions of (A) AuNR-CTAB, (B) AuNR-(PAA PAH) and (C) AuNR-(PAA PAH GG) and the respective UV-Vis spectra were acquired after an overnight; (D) Absorbance as a function of salt concentration. For each type of particle, absorbance was measured at maximum wavelength found on particles without salt..... 27

Figure 17 - UV-Vis spectrometry analysis of pH influence on particles stability. Defined concentrations of HCl and NaOH were added to solutions of (A) AuNR-CTAB, (B) AuNR-(PAA PAH) and (C) AuNR-(PAA PAH GG) in order to get acidic and basic conditions, respectively. The respective UV-Vis spectra were acquired after an overnight; (D) Absorbance as a function of pH. For each type of particle, absorbance was measured at maximum wavelength found on particles at pH=6. 28

Figure 18 – Cell viability of SaOS-2 after 24 hours, with different types of particles at 0.08 nm and 0.04 nM. 29

Figure 19 - Cell viability of SaOS-2 cell line cultured with AuNR, AuNR-(PAA PAH) and AuNR-(PAA PAH GG) for 14 days, comparing to control; Upper panel it is a general view of all data. The inferior one represents the same data but organized by particles type. From left to right: cell viability when incubated with AuNR, AuNR-(PAA PAH) and AuNR-(PAA PAH GG). Results expressed as an average ± standard deviation. (n=9, * $p<0.01$; ** $p<0.001$). 30

Figure 20 - Cell Viability of ASC cultured with AuNR-(PAA PAH GG) for 1, 7 and 14 days, comparing to cell viability of ASC without particles. Results expressed as an average ± standard deviation. (n=6). 31

Figure 21 - Fluorescence microscopy of SaOS-2 incubated without particles (A) and with AuNR-(PAA PAH GG) (B) for 48 hours. Red areas represent the cytoskeleton stained by Texas Red – X phalloidin and blue areas the nuclei, stained with DAPI; dark filed microscopy of the same samples (C) and (D) respectively..... 32

Figure 22 - TEM images of SaOS-2 after 14 days of incubation with AuNR-(PAA PAH GG) at 0.05 nM. AuNR-(PAA PAH GG) aggregated within cytoplasmic vesicles, shown with arrows. Magnification of 40 000X (left) and 60 000X (right). 32

Figure 23 - TEM images of rabbit ASC after 14 days of incubation with AuNR-(PAA PAH GG) at 0.05 nM. AuNR-(PAA PAH GG) aggregated within cytoplasmic vesicles, shown with arrows. Magnification of 1 200X (left) and 50 000X (right). 33

Figure 24 – UV-Vis spectra of AuNR-(PAA PAH) (A) and AuNR-(PAA PAH GG) (B) after loading with dexamethasone. In both graphs, the black line is the UV-Vis spectra of particles before washing; while the red line represents the UV-Vis spectra of particles after one wash cycle..... 33

Figure 25 – UV-Vis spectra of Dexamethasone (black line) and Gellan Gum (red line)..... 34

Figure 26 - FTIR spectra of (A) dexamethasone; (B) AuNR-(PAA PAH GG); (C) dexamethasone loaded AuNR-(PAA PAH GG)..... 35

List of Tables

Table 1 Comparison of High Acyl and Low Acyl Gellan Gum properties [66, 79]. 12

- This page was intentionally left blank. -

Glossary

A
ASC – Adipose derived stem cells
AuNP – Gold nanoparticles
AuNR – Gold nanorods

B
BSA – bovine serum albumin

C
CTAB – Cetyl trimethylammonium bromide

D
DAPI – 4',6-diamidino-2-phenylindole
DDS – Drug delivery systems
Dexa – Dexamethasone

E
EBSD - Electron Backscatter Diffraction

F
FTIR – Fourier transform Infrared spectroscopy

G
GG – Gellan gum

I
IR – Infrared

L
LbL – Layer-by-layer
LPB – Longitudinal plasmon band

N
NIR – Near Infrared
NP – Nanoparticles

O
OD – Optical density

P
PAA - Poly(acrylic acid sodium salt)
PAH - Poly(allylamine hydrochloride)
PDDAC - Poly(diallyldimethylammonium chloride)
PE – Polyelectrolytes
PEI - Polyethyleneimine
PSS – Poly(styrenesulfonate)

S
SEM – Scanning electron microscopy
SPR – Surface plasmon resonance

T
TEM – Transmission electron microscopy
TRITC - Tetramethylrhodamine B isothiocyanate

Chapter 1

Introduction

1.1. Gold Nanoparticles

Metal nanoparticles exhibit unique physicochemical properties, different from the corresponding bulk material, which are a direct consequence of the quantic effect [1]. Among the different types of metal nanoparticles, gold nanoparticles (AuNP) have arisen a lot of interest between researchers of different fields [2]. Drug delivery, biosensing, bioimaging and photothermal therapy are some of the areas where these particles can be applied [2–7]. Along with its straightforward synthesis process and easy functionalization, AuNP outstand from the other metallic counterparts because of their non-toxic nature and biocompatibility. Furthermore, these particles offer a multitude of advantages for biological applications [6, 8]. Firstly, one can consider the ability to tune size and shape of particles in a wide range. Gold nanoparticles can be synthesized with different shapes namely, spheres [9], rods [3, 5, 7], cages [4] and star-like [10]. The high surface to volume ratio provides an efficient loading of multifunctional moieties and enhances solubility and stability of the loaded drugs, which is desirable for therapeutic approaches.

Similarly to other noble metal nanoparticles, AuNP can absorb light of several wavelengths due to the formation of plasmon resonances on their surface. These surface plasmon resonances (SPR) represent the collective oscillation of the conduction electrons, caused by the resonant excitation via the incident photons. The surface electron density is polarized to one side as the wave front of light passes, leading to a standing oscillation in resonance with light frequency [11]. The intensity and wavelength of SPR bands are directly influenced by particle size and shape, the solvent, surface ligand, core charge, temperature and proximity of other nanoparticles [11–13]. AuNP also have the capability to convert the absorbed light into heat. In this sense, AuNP can be used as cell imaging label and as photo-thermal agent for controlled drug release and/or cancer ablation by hyperthermia [14]. The possibility to combine those advantages in a single device paves the way for the development of theranostic nanoscale systems.

1.1.1. Gold Nanorods

Anisotropic gold nanorods (AuNR), as an alternative to spherical nanoparticles, display two different SPR bands, one related to their width - transverse SPR band - and the other related to length, the longitudinal SPR band (LPB) (Figure 1). While the first appears near 500 nm, and does not depend on the aspect ratio of NP, the wavelength of the LPB can be tuned according to AuNR size and aspect ratio [11]. As the aspect ratio (length divided by width) increases, an increase on intensity and wavelength maximum of the LPB is noticed. Then, this band can be anywhere from the visible (600 nm) to the near Infra-Red (NIR) (>1100 nm) [15]. The capacity of absorbing in the NIR zone is extremely useful for biomedical and regenerative medicine applications because NIR light has minimal absorption by skin and tissues. Therefore, it allows the development of devices with deeper tissue penetration and minimal tissue invasion [14, 16], namely for hyperthermia therapy and drug/gene delivery [5] and NIR-resonant biomedical imaging modalities [14]. These includes two-photon luminescence imaging [4, 17, 18], photoacoustic tomography [16, 19], optical coherence tomography [20–22] and X-ray computed tomography.

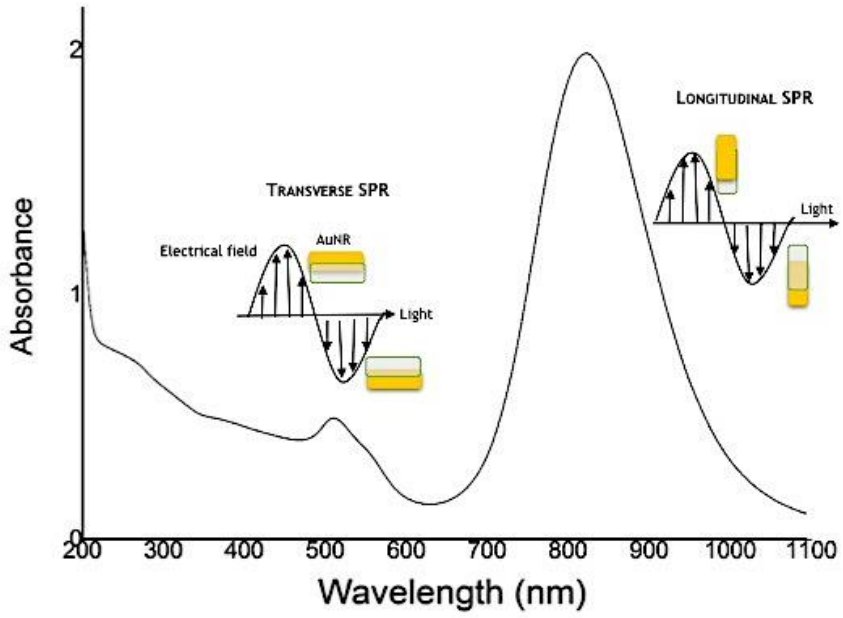

Figure 1 – Typical UV-Vis spectrum of AuNR, with schematic representations of SPR in AuNR.

Hence, as other shapes of AuNP, AuNR can be used for a multitude of imaging and therapeutic modalities. These can be fused in one single system to combine both therapeutic and diagnostic capabilities, following the concept of theranostics. Moreover, the possibility to remotely mediate the functional modalities by NIR-light confers to AuNR an exceptional advantage over other nanoparticle-based theranostic platforms.

Gold Nanorods Synthesis

In terms of NP synthesis, the kinetically and thermodynamically favourable morphology is the spherical shape. Then, to form non-spherical particles it is necessary to direct the nanoparticles growth into an anisotropic dimension, breaking the natural tendency for isotropic growth. To date, numerous methods regarding AuNR synthesis have been reported, as reviewed by Vigderman *et al.* [15] and P. Zhao *et al.* [1]. The first reported protocols were based in electrochemical and photochemical reduction reactions, both in aqueous surfactant media and nanoporous templates [23]. However, such procedure had some weaknesses, such as the low total yield of the procedure. In 2001, Murphy's group developed a seed-growth mediated method [24], which was improved in 2003 by El-Sayed's group [25]. So far, this wet-chemical synthesis is known to be the most favourable one, since it is possible to prepare solutions of well-defined and monodispersed AuNR in high yields.

The seed-mediated growth method (Figure 2) relies on the chemical reduction of a chemical gold source (chloroauric acid, $HAuCl_4$) by a weak reducing agent, ascorbic acid [24]. Such reaction leads to the formation of 3-4 nm AuNP, which are used as seeds. Then, these seeds are added to a growth solution, containing the chloroauric acid, freshly prepared ascorbic acid and CTAB as surfactant. CTAB selectively forms a tightly packed bilayer on the side faces of particles, meaning that the ends of the rods stay more exposed, allowing the anisotropic growth along the longitudinal axis. As a result, spherical seeds can undergo a surfactant-mediated growth leading to AuNR formation. One of the improvements proposed by El-Sayed's group took into account the large amount of spherical AuNP and AuNP with other shapes formed as by-products in the first described protocol [25]. To overcome this problem, the group proposed the use of borohydride-capped seeds, instead of the citrate-capped seeds used by Murphy's group. Moreover, silver nitrate was added to the growth solution, in order to control the aspect ratio of AuNR. Such modifications increased the final yield of the reaction and led to AuNR with aspect ratios between 1.5 and 4.5, with only traces of spherical AuNP. Before use, particles should be washed in order to remove the large CTAB excess that remains in solution.

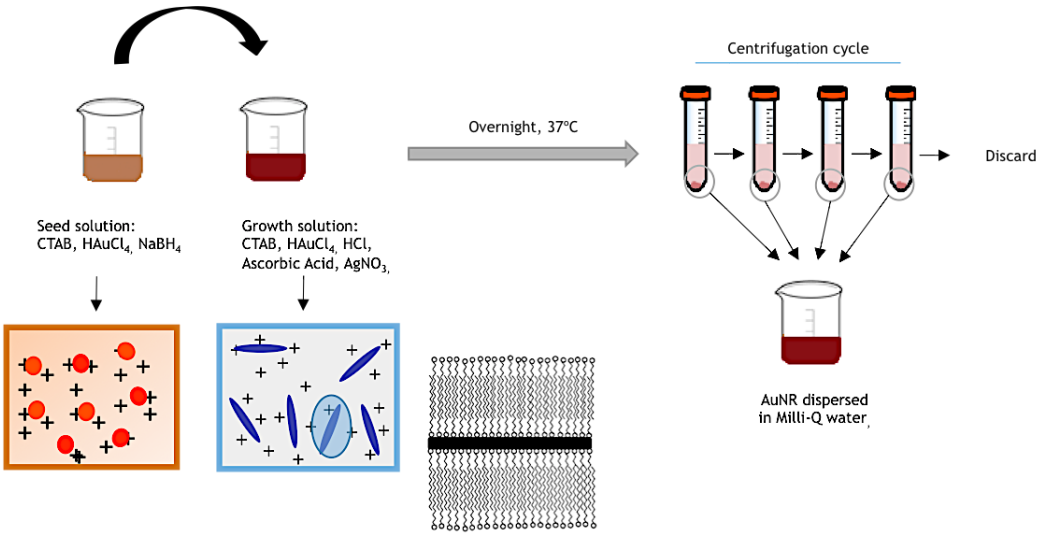

Figure 2 - Schematic representation of AuNR synthesis process.

Gold Nanorods Cytotoxicity and Surface Modifications

Prior gold nanoparticles wide application in medicine, it is necessary to understand the *in vivo* and *in vitro* cell viability when cells are exposed with the material. Whereas a multitude of studies have already addressed this key point, the results are not consensual, which is probably a consequence of the lack of standardized protocols, with well-established concentrations of particles and cell types [14, 26, 27]. Therefore, cytotoxicity assays have to be performed with the prepared nanoparticles for the intended applications.

Some works appointed particles size as an important factor for AuNP toxicity, mostly due to the increased redox-reactivity found in small particles (d_{core} < 2 nm) [28, 29]. Y. Pan *et al* [28] have performed a systematic cytotoxicity study of water-soluble AuNP stabilized by triphenylphosphine derivatives, with sizes ranging from 0.8 to 15 nm. Particles were incubated with four different cell lines, representing the major functional cell types. The AuNP cytotoxicity has shown to be highly size-dependent, since smaller particles induced cell death. However, cell viability was not affected by the ligand chemistry. Recently, Vijayakumar *et al*. [29], have performed a similar study using citrate-capped AuNP. Interestingly, the cell viability test shows two distinguishable cytotoxic effects. The AuNP of 3 nm, 8 nm, and 30 nm after 24 hours of incubation were cytotoxic, whereas particles of 5 nm, 6 nm, 10 nm, 17 nm, and 45 nm were non-toxic, even with higher concentrations and long-term exposure. With these results, the authors have concluded that AuNP exert only a mild toxicity or in some cases no toxicity at all in MCF-7, PC-3, and CHO22 cell lines.

Besides the size-dependent toxicity reported to spherical AuNP, recent works show evidences that AuNR cytotoxicity is independent of particles aspect ratio, but highly dependent of its surface chemistry [30, 31].

The aforementioned seed mediated method for AuNR synthesis uses CTAB as a structure-directing agent. This surfactant forms a chemisorbed bilayer, which coats the AuNR surface. As a result, CTAB bilayer also prevents particles aggregation under certain conditions due to the repulsive electrostatic interactions between the cationic groups. Nevertheless, the presence of free CTAB molecules have shown clear cytotoxic effects, due to their interactions with the cellular membrane, weakening membrane integrity [31].

To improve biocompatibility and stability in biological media, and then allow biomedical applications of AuNR, particles need to be properly purified and functionalized. Therefore, several groups have been focussed their work in the development of new processes of surface modifications [14, 15], by replacing and/or masking the CTAB adsorbed on AuNR surface.

The most used methods are schematically represented in Figure 3.

Method A: A Layer-by-layer (LbL) approach was first suggested by Murphy *et al*. [32], and relies on the successive multilayer coating of anionic and cationic polyelectrolytes on the AuNR surface (Figure 3-A). The strategy consists on the adsorption of anionic polyelectrolytes such as polyacrylic acid (PAA) or polystyrenesulfonate (PSS) on the positively charged AuNR-CTAB, due to electrostatic interactions. As a result, the AuNR net charge changes from positive to negative, and cationic polyelectrolytes can then be adsorbed. Poly(diallyldimethylammonium chloride) (PDDAC) [31] and poly(allylamine hydrochloride)

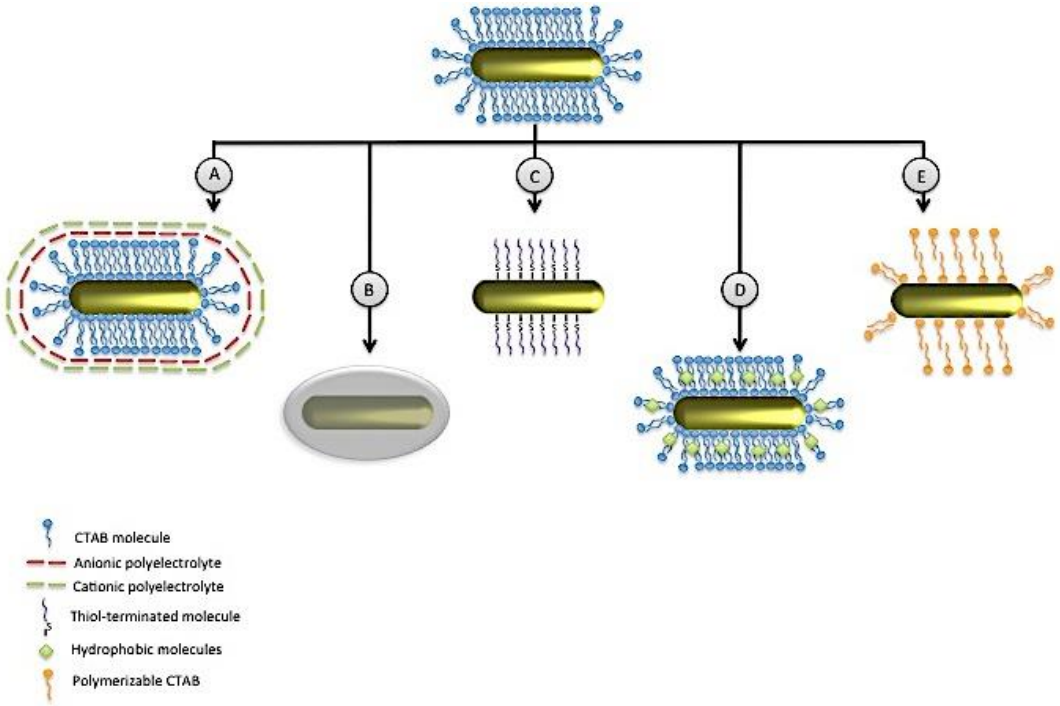

Figure 3 - Common methods of AuNR surface modification: A-layer by layer; B – silica coating; C – displacement of the surfactant by thiol-terminated molecules; D – insertion of hydrophobic molecules; E – on-particle polymerization.

(PAH) [32, 33] are some of the polymers commonly used for cationic coating. This process can be repeated multiple times, improving AuNR stability and allowing the incorporation of cargos with different charge. Adsorbed polyelectrolytes hinder desorption of CTAB molecules, leading to a decrease of AuNR cytotoxicity [33]. Moreover, contrarily to CTAB-coated AuNR, polyelectrolyte-coated AuNR displayed an improved solubility in solutions with high salt concentration, polar organic solvents and biological media, which is necessary for biological applications [15]. For example, AuNR modified with PAA and PAH have shown 90% of cell viability after four days, whereas CTAB one reduce the cell viability to 40% [33]. This fact confirms that free CTAB molecules are greatly contributing for the observed AuNR cytotoxicity and not its charge or size.

Method B: Replacing CTAB by other molecules, with reduced cytotoxicity, is also possible. To do so, some groups have used mesoporous silica to coat AuNR [34–37], resulting in a core-shell nanoparticles structure (Figure 3-B). The preferred method, an adaptation of Stöber method for silica coating, makes use of the CTAB bilayer on AuNR surface as a template. Consequently, three-dimensional polymerization of the silica precursor, tetraethyl orthosilicate (TEOS), occurs on the surface of CTAB molecules, leading to silica condensation. In the end of the process, the surfactant is completely removed by several washes with ethanol and through ion change, which can ensure particles non-cytotoxicity. Due to its morphology, comprising several mesopores and nanochannels, mesoporous silica is usually synonym of high payload of drug/genes, which is very useful for drug delivery systems (DDS) [38]. Therefore, besides improving AuNR biocompatibility, such approach empowers AuNR as a drug delivery system. Nevertheless, mesoporous silica coated AuNR are described as biocompatible, Zhu *et al*. has reported notable cytotoxicity when those particles were incubated with several cell lines [39].

Method C: One of the standard methods for AuNP modification is based on its high affinity with thiol moieties, arising from a strong S-Au bond [40]. This type of linkage is sufficient to prepare stable AuNP conjugates. Therefore, they can be easily and directly functionalized on its surface with different biomolecules containing sulfur groups, with CTAB being displaced by excess of thiolated species, (Figure 3-C). The most common surface ligand is the thiolated polyethileneglycol (PEG), which can minimize particles cytotoxicity while improving its stability in physiological media [41–43].

Insertion of hydrophobic molecules within the CTAB bilayer (Figure 3-D) [27] hinders the release of CTAB molecules from AuNR surface to the media, thus improving particles biocompatibility. As depicted in Figure 3-E, the use of polymerizable surfactants [44] can also allow to obtain AuNR with reduced cytotoxicity. These surfactants can polymerize on-particle, which decreases surfactant desorption from the surface of nanoparticles. Consequently, particles became more biocompatible and stable under different processing steps as centrifugation or dialysis.

1.1.2. Gold Nanoparticles as DDS

The impact of nanotechnology on the development of new drug delivery systems (DDS) is a breakthrough, and various types of NP have been developed in order to improve drug delivery [45]. NP with encapsulated, dispersed, adsorbed or conjugated drugs, have unique characteristics that can improve the drug delivery process. Nanocarriers often enhance the drug solubility, leading to rapid dissolution, which results on an improved bioavailability. The drug dose needed to achieve therapeutic benefit can be potentially reduced, since the delivery is more efficient when nanomaterials are used. Thereby, application of NP as DDS could also improve therapeutic efficacy, reduce drug dose and re-dosage needs while avoiding the deleterious side effects of drugs. Furthermore, NP size and surface characteristics can be easily manipulated to achieve both passive and active drug targeting [45]. The therapeutic applications of NP are wide-ranging, such as cancer treatment [46], vaccine delivery [47], and gene therapy [48], among others.

AuNP facile synthesis, easy surface modification and bioconjugation, chemical inertness, excellent biocompatibility and low cytotoxicity are characteristics that made these particles a proper vehicle for DDS, as recently reviewed by Kumar *et al.* [49] and Jeong *et al.* [50]. Moreover, their high surface area and ability to be functionalized with a variety of biomolecules allow to greatly increase the amount of immobilized biomolecules.

Nevertheless, the application of AuNP as DDS implies the engineering of its surface, in order to provide an effective and stable immobilization of the load to AuNP surface. Upon surface modification, particles can be conjugated with several types of molecules such as peptides [51], proteins [52], small drugs [53], plasmid DNA (pDNA) or small interfering RNA (siRNA) [50]. Drug loading on AuNP can occur by various methods. As aforementioned, one of the most used strategies to functionalize AuNP makes use of thiolated species, which strongly bind to AuNP surface. Thiolated DNA [54] and thiolated peptides [55] anchor to the particles via S-Au bonding, making AuNR biocompatible vehicles for drug and gene delivery. Thiol motifs can also be used to act as linker between a desired molecule and AuNP surface. As an example, Zandberg *et al.* [56] developed a photothermal release system, where a linker with alkanethiol and oxabicycloheptene motifs were used to tether a fluorescent dye to AuNP

surface. While the alkanethiol motif can act like an anchor, the latter is responsible for the photoresponsible properties of this system. A temperature above 60ºC-70ºC leads to bond breaking of oxabicycloheptene and consequently release of its cargo (Figure 4).

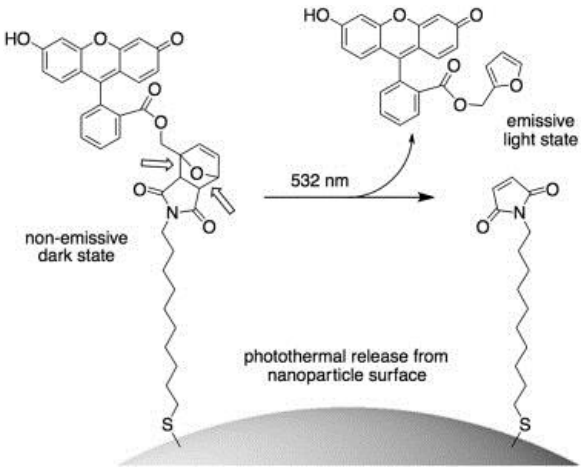

Figure 4 – Schematic representation of Zandberg's rational [56].

Another strategy for drug loading is to modify AuNP core with mesoporous silica shell (AuNR-SiO_2). As stated before, mesoporous silica is highly porous, leading to a high drug payload. By instance, Zhang *et al*. [37] have designed a hybrid strategy taking advantage of mesoporous silica and AuNR properties. The group incorporated an anti-cancer drug, doxorubicin, within the silica shell and its release was controlled via application of NIR light. Monem and colleagues [35] have used a similar approach to load into AuNR- SiO_2 and deliver doxorubicin both *in vitro* and *in vivo*. The formulation was found to possess a very low toxicity effect in normal tissue and could target its full damage to cancerous tissues.

Likewise, Minati *et al*. [57] incorporated doxorubicin on gold nanoparticles surface by adsorption, followed by a LbL deposition of polyelectrolytes. In acidic conditions, such as those found in tumours and endocytic vesicles, doxorubicin amino groups are highly protonated and the polymeric shell collapses. Consequently, doxorubicin is rapidly released at acidic pH, comparing to neutral conditions. These NP were able to deliver its cargo into the nuclei of A549 cells, leading to pronounced cytotoxic effects to lung tumour cells. Elbakry *et al*. have successfully designed layer-by layer assembled AuNP for intracellular delivery of DNA [58] and siRNA [59]. The strategy was to intersperse the genetic material within PEI layers, as shown in Figure 6.

AuNP also offer the possibility to combine multiple functions, such as drug delivery and imaging [14]. Hence, researchers had explored AuNP not only as a therapeutic tool but also as an imaging probe, which can give meaningful knowledge about NP fate after administration and serve as a theranostic device.

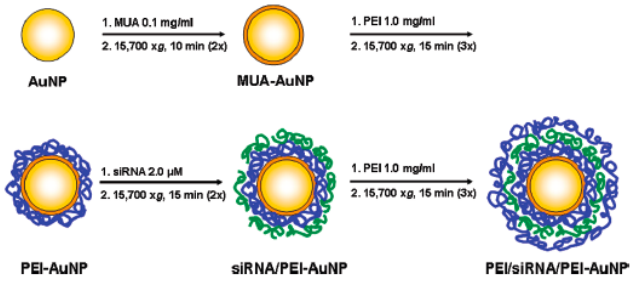

Figure 6 - Flowchart of Elbakry *et al.* strategy for the production of layer-by-layer assembled AuNP for siRNA delivery [59].

When comparing to spherical AuNP, non-spherical nanoparticles may have some advantages as a multifunctional DDS. The possibility to absorb light in the NIR region can be exploited and confer new functionalities for DDS. For instance, controlled drug release can be achieved taking advantage of AuNR photothermal effects. Figure 5 schematically represents the aforementioned strategy. When AuNR absorbs NIR light, energy is dissipated as heat, which can help the release of drugs that are physically absorbed or chemically conjugated to AuNR surface. Following this rational, Wijaya *et al.* designed a system where two different DNA oligonucleotides were separately attached and selectively released from a mixture of two different AuNR. The application of different NIR laser, corresponding to the LPB maximum wavelengths of each type of AuNR, confers the selectivity to this system [60].

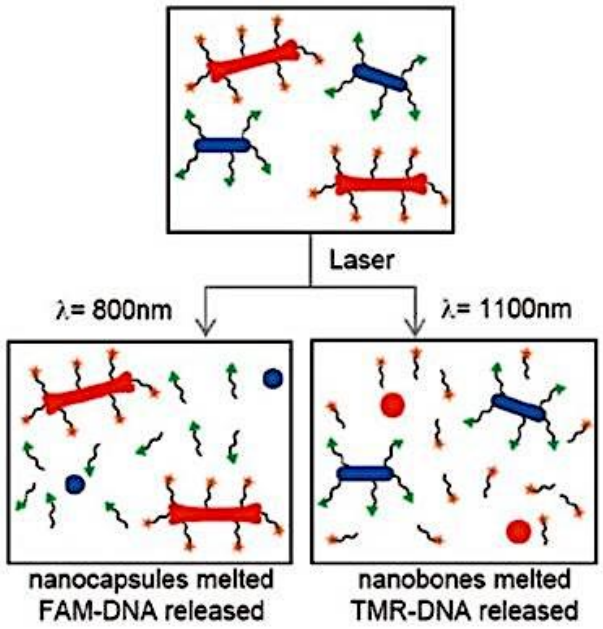

Figure 5 - Schematic representation of Wijaya *et al.* rational. Selective releases were induced by selective melting of gold nanorods *via* ultrafast laser irradiation at the nanorods' LPB resonance peaks. When particles were submitted to an 800 nm irradiation (left), AuNR (blue) melts and release its cargo, DNA labelled by FAM (green triangles). Exposure to an 1100 nm irradiation (right) melt the nanobones (red), which selectively release DNA labelled with TMR (orange stars). Releases were efficient (50–80%) and externally tunable by laser fluence. Released oligonucleotides were still functional [60].

Moreover, AuNR were employed to deliver an innate immune activator (5'PPP-single stranded RNA, ssRNA) against type A influenza virus [61]. ssRNA were conjugated with AuNR via electrostatic interactions and applied in human respiratory bronchial epithelial cells infected with the virus. The AuNR optical properties were advantageous for this work, enabling the observation of internalized particles by dark field microscopy. By its turn, Guo *et al*. used chitosan-AuNR as a multifunctional system for cell imaging, drug delivery and NIR-photothermal therapy [5]. AuNR were coated with a chitosan matrix, which was used as a reservoir for the loading of cisplatin. The *in vitro* experiments have shown that modified nanoparticles were able to deliver the drug in the intracellular compartment. Moreover, due to AuNR optical properties, AuNR can be used as labelling probes, allowing real-time cell imaging by dark-field microscopy. In a recent work, Chen *et al*. [62] described a method to stabilize AuNR with polyelectrolytes (PE) and BSA protein to obtain multi-layered AuNR (AuNR-PE-BSA). Doxorubicin was then encapsulated into AuNR-PE-BSA by electrostatic interactions and particles were successfully used for *in vivo* combined thermo-and-chemo-therapy.

The possibility of combining several functionalities in only one system is really advantageous for DDS. Beneficial synergies that can be achieved without the administration of adjuvants, the improved control over the system and the possibility to obtain more in-depth information about the fate of the carriers are absolutely desired under this scope. AuNP, including AuNR, are increasingly being used as DDS surpassing other inorganic nanoparticles, like quantum dots or carbon nanotubes, mostly due to their biocompatibility and inherent physicochemical properties.

- This page was intentionally left blank. -

1.2. Gellan Gum

Due to their unique properties, biocompatibility, low production costs and widespread ability, natural gums are being used in several applications. These polysaccharides started to be applied in food industry, as a structuring and gelling agent in a variety of food products [63]. Nowadays, they can be found on several personal care products, for example toothpastes and sunscreens, and as excipients for pharmaceutical and biomedical purposes [64].

Gums can be extracted from numerous sources, like plant tissues, seeds, seaweeds and microorganisms. Among the bacterial polysaccharides, gellan gum (GG) is the most well-known. GG is a nontoxic, biocompatible and biodegradable anionic heteropolysaccharide secreted by the bacteria *Sphingomonas elodea* (previously *Pseudomonas*) [65]. Its molecular structure is based in one repeating unit consisting of α-L-rahmnose, ß-D-glucose and ß-D-glucuronate, in the molar ratios 1:2:1 [67–69]. In the native form, or high acyl form, two types of acyl substituents are present: acetyl and L-glyceryl [69]. As shown in Figure 7, both substituents are located on the same glucose residue. However, while L-glyceryl is present, on average once per repeat, acetyl appears once per two repeating units [70]. Low acyl gellan gum is obtained through alkaline hydrolysis of native GG, which removes both of the acyl residues [65].

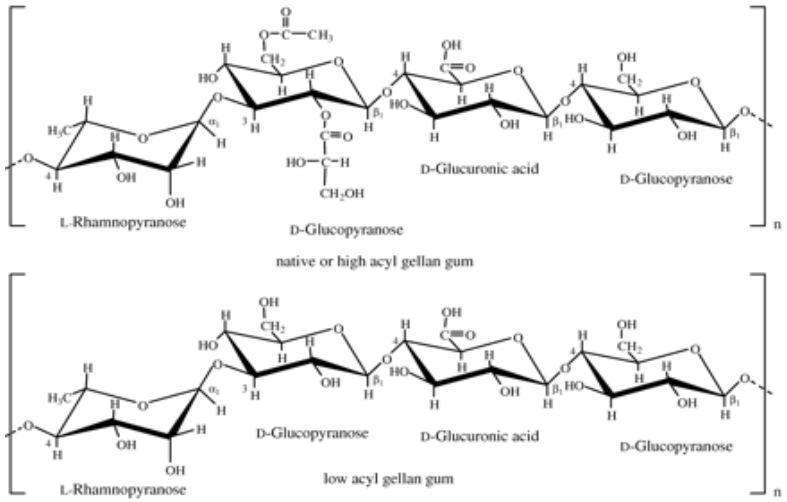

Figure 7 - Gellan gum structure. Native or high acyl gellan gum (upper image); low acyl gellan gum (image bellow) [108].

At high temperatures, gellan has a disordered coiled conformation. But as the temperature decreases, polymer chains start to fold into double helix structure (Figure 8) [71]. At this configuration, gellan can exhibit "weak gel" characteristics, though is not considered a true gel. Both forms of gellan form hydrogels in the presence of mono, di- [72], [73] and trivalent ions, and gel characteristics are influenced by the presence of acyl groups [74]. In high-acyl gellan gum, the acyl residues are located on the periphery of the helix, obstructing the polymer chain association. Thus, packing is less effective and the resulting gels are soft, elastic and non-brittle. In contrast, low-acyl gellan gum produces firm, non-

elastic, brittle gels since ions can easily link polymer chains and form a branched network. Differences between high acyl and low acyl gellan gum are stated on Table 1. Other gel properties like gelling temperature, gel strength and rate of gel formation depend on several factors of the prepared solution, such as pH value [75], type and concentration of ions [76] and presence of sugars [77].

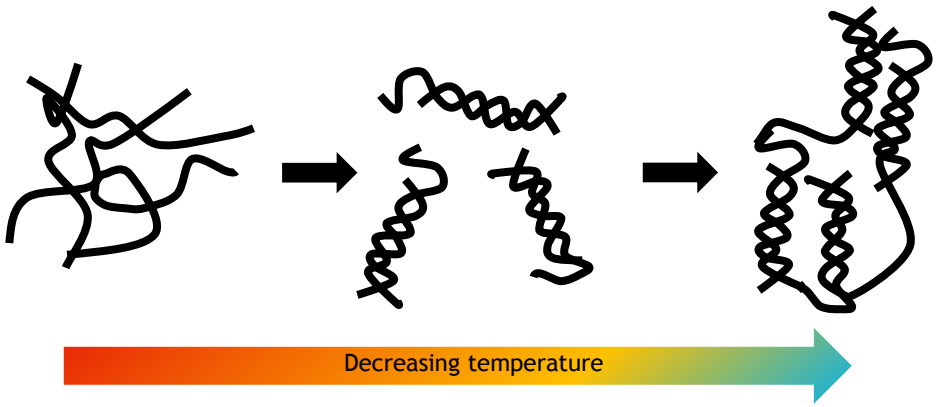

Figure 8 - Schematic representation of gradual transformation of GG in aqueous solution, through different temperatures. Adapted from [64].

Table 1 - Comparison of High Acyl and Low Acyl Gellan Gum properties [66, 79].

	High Acyl Gellan Gum	Low Acyl Gellan Gum
Molecular weight	1-2x10^6 Daltons	2-3x10^5 Daltons
Solubility	Hot water	Hot or cold water
Set temperature	70-80ºC	30-50ºC
Thermo reversibility	Thermo-reversible	Heat stable

As a product, GG is approved for food, non-food, cosmetic and pharmaceutical use in numerous countries, including the United States and the European Union [53]. Applications of GG for tissue engineering [65, 80-83], dental care [83], gene delivery [85, 86] are also being studied.

1.2.1. Gellan Gum in Nanotechnology

To date, GG has been widely used in pharmaceutical applications, and various strategies for regenerative medicine, stomatology and gene transfer technology are under development [64]. However, few investigations have reported the use of GG for nanoparticles development. In 2008, Dhar *et al.* [53] reported the synthesis of AuNP using GG as capping and reducing agent. These particles have shown a superior stability to pH alterations and

addition of electrolytes, comparing to the particles prepared by the standard methods using citrate or borohydride as reducing agent. Additionally, particles were successfully loaded with doxorubicin hydrochloride, an anticancer drug, for drug delivery purposes. Later, the same group accessed the cellular uptake of gellan gum-reduced AuNP (AuNP-GG) in mouse embryonic fibroblast cells and human glioma cell line [86]. After three hours of treatment with AuNP-GG, results have shown that cancer cells uptake AuNP-GG, contrarily to fibroblast cells. This work also evaluated AuNP-GG cytotoxicity in rats after a treatment of 28 days with an orally delivered dose of particles. After the treatment, rats did not show biochemical or haematological alterations, meaning that AuNP-GG particles were non-toxic in animals following oral administration. In a different study [87], a glycolipid – sophorolipid – was successfully conjugated with AuNP-GG and loaded with doxorubicin to increase cytotoxic effect against cancer cell lines. Likewise, the same group have extended their process to silver NP [88]. Recently, Sivakumar and colleagues used GG to coat magnetic NP [89]. This approach led to biocompatible particles with low cytotoxicity, with potential for drug delivery applications.

GG combined with polyethyleneimine (PEI), a widely known transfection agent, have been developed for gene delivery purposes [84]. The GG-PEI nanoparticles have shown to enhance transfection efficiency and to minimize the cytotoxicity as compared to PEI, or other commercial transfection agents. The authors claim that this is due to a partially neutralization of PEI positive charge by GG, which also protects plasmid DNA from nucleases and serum proteins present in the blood.

- This page was intentionally left blank. -

1.3. Aim of the Project

After literature overview, it is possible to state that AuNR show a great potential as DDS. Their ease of synthesis and functionalization, biocompatibility and optical properties make them a promising tool not only as a carrier for drug delivery but also for cell tracking applications. Since the preparation of AuNR involves the use of cetyl trimethylammonium bromide, a cytotoxic surfactant, their surface modification is essential to render them biocompatible. Therefore, several methods including thiol chemistry, shell coating (e.g., silica, chitosan) and LbL coating have been proposed.

This work aims to develop gellan gum-coated AuNR, to be used as DDS in tissue engineering and regenerative medicine approaches.

Gellan gum is a biocompatible natural gum with great physicochemical properties and has been widely used for food, pharmaceutical and biomedical applications. Nevertheless, there are only few reports regarding the application of this heteropolysaccharide in nanotechnology. To our knowledge, only Dhar's group [53] has used GG as reducing and stabilizing agent to produce gold nanoparticles for further drug loading. Furthermore, no specific investigation has been reported regarding on the coating of AuNR with gellan gum shell. This shell would assure particles biocompatibility and increase their stability, under different conditions.

Merging the advantages of both compounds AuNR and GG, herein it was designed and characterized a novel methodology for AuNR functionalization. The proposed strategy involved two steps: i) pre-coating via adsorption of two different polyelectrolytes (PAA and PAH) using a LbL strategy, and ii) formation of a GG shell at the gold core surface. To analyse the feasibility of this approach, nanoparticles were analysed through different methods, in order to assess their optical properties, size, dispersion, surface charge and morphology. To validate our particles for further biomedical applications, *in vitro* studies were performed with two different cell-types: SaOS-2, human osteoblast-like cells, and rabbit adipose derived stem cells. These analysis aims to determine particles cytotoxicity and to evaluate the cellular uptake.

Even though, the first step of the work was aimed to assess the feasibility of the methods for obtaining core-shell structure of AuNR-GG, the second major goal comprised the incorporation of a model drug used in bone tissue engineering.

Recently, some reports highlighted the possibility that AuNP stimulate the osteogenic differentiation of mesenchymal stem cells as well as osteoblast-like cell, toward osteoblast formation. Yi *et al.* [90] have reported that 20 nm AuNP induce mechanical stress on the mesenchymal stem cells, which activates p38 mitogen-activated protein kinase pathway (MAPK) signalling pathway. This signalling pathway regulates the expression of relevant genes that induce osteogenic differentiation and inhibits adipogenic differentiation. Zhang *et al.* [91], in a recent work, found that 20 nm and 40 nm AuNP have a beneficial effect on cell viability, differentiation and mineralization of mice osteoblasts. These effects were more noticeable in cells treated with smaller AuNP. The authors also found that such biological effects occur via the ERK/MAPK signalling pathway. In another work, Liu *et al.* [92] have

investigated the size effect of gold nanoparticles on the proliferation, differentiation and mineralization of a murine pre-osteoblast cell line, MC3T3-E1, *in vitro*. After 7 and 14 days of culture, proliferation, differentiation, and mineralization of MC3T3-E1 cells was reported, in a time- and dose-dependent manner. Better results were observed with smaller particles, suggesting that the size may play a role to stimulate the osteogenic differentiation. Contrarily, Tsai *et al*. [26] reported that 10 nm AuNP do not affect osteogenesis and apoptosis of MG63 osteoblast-like cells. They observed that the viability, specific nodule-like phenotype and gene expression were similar with or without particles. Also, the apoptosis and necrosis percentages of the untreated and treated cells after 8 days were similar.

Therefore, herein it was hypothesised a new methodology to combine AuNR biocompatibility, optical properties, drug delivery capacity and regenerative potential. To that end, and following the rational of Oliveira *et al*. [93] and Monteiro *et al*. [94], dexamethasone was loaded inside polyelectrolyte-coated AuNR (AuNR-(PAA PAH)) and GG-coated AuNR (AuNR-(PAA PAH GG)) in order to compare their feasibility as drug delivery systems.

Thereby, this work assumes a relevant role on the conception of new integrated systems of drug delivery and imaging. With this approach, it was possible to understand the characteristic of modified AuNR and how they interact with cells, providing important data for future studies.

1.4. Outline

This document is divided into five chapters. In **Chapter 1 – Introduction,** a general view of the scientific background supporting this project and its objectives is presented. The materials, methodologies and equipment are described in **Chapter 2 – Materials and Methods**. **Chapter 3 – Results** – encloses all the relevant results found during this project. The results and their implications are further discussed and analysed in **Chapter 4 – Discussion**. As a final point, the main results are highlighted in **Chapter 5 – Conclusions** – as well as the prospects and future work.

Chapter 2

Materials and Methods

2.1. Synthesis of Gold Nanorods

The gold nanorods were synthesized by the seed-mediated growth method [25]. First, a gold seed solution was prepared by the borohydride reduction of 0.25 mM $HAuCl_4$ (Sigma-Aldrich) in an aqueous 0.2 M Cetyltrimethylammonium bromide (CTAB) (Sigma-Aldrich) solution. Subsequently, 100 µL seed solution was added to a 21.6 mL growth solution containing 0.2 M CTAB, 1.15 mM $HAuCl_4$, 56 mM of HCl (VWR), 2.3 mM ascorbic acid (Sigma-Aldrich) and 0.23 mM silver nitrate (Sigma-Aldrich). The solution was aged for 24 hours at 30ºC to ensure the complete formation of AuNR. CTAB excess was removed by three cycles of centrifugation (5,000rpm, 8,000rpm, 10,000rpm and 13,500rpm for 15 minutes each) and particles were dispersed in Milli-Q water. The concentration of gold nanorods was determined at the LPB peak maximum using molar extinction coefficient $\varepsilon = 5.10^9\ M^{-1}\ cm^{-1}$ [95].

2.2. Surface Functionalization

2.2.1. Functionalization with PAA and PAH

Purified particles were modified using a layer-by-layer approach. Briefly, a solution of 1.60 nM of particles was added, drop-wise and under vigorous stirring, to an aqueous solution of poly(acrylic acid sodium salt) (PAA) (4 g/L, Mw 5 100 Sigma-Aldrich; 6 mM NaCl). PAA adsorption was allowed to proceed for 2 hours, at room temperature and under stirring. PAA excess was removed by centrifugation and particles re-dispersed in Milli-Q water. The process was repeated with poly(allylamine hydrochloride) (PAH) (4g/L, Mw 15,000 Sigma-Aldrich; 6mM NaCl). After, particles were washed by centrifugation.

2.2.2. Functionalization with GG

Low acyl gellan gum (Gelzan™ CM Gelrite®, Sigma-Aldrich) solution was prepared with a concentration of 0.5% (w/v), in ultra-pure water. To allow its dissolution, GG solution was heated up to 90ºC, under vigorous stirring. Then, AuNR modified with PAA and PAH were

added, drop-wise, and the solution was continuously heated and stirred for 5 minutes. The mixture was cooled down at room temperature, being stirred overnight. Finally, particles were washed by centrifugation.

2.3. Characterization of nanoparticles

2.3.1. Spectrophotometric analysis (Optical properties)

All AuNR solutions were appropriately diluted and absorbance from 1100 to 200 nm wavelength was determined using a UV-Vis spectrophotometer (Shimadzu, UV-1601). UV-Vis analysis was used to confirm the rod shape of AuNR and to determine its concentration. The extinction coefficient, ε =5.10^9 M^{-1} cm^{-1} was used to determine the particles concentration, according to the Beer-Lambert equation (1) [95].

$$Abs_{\mathrm{LPB}} = \varepsilon lc \qquad (1)$$

where Abs_{LPB} corresponds to the maximum absorbance value of LPB, l corresponds to the length of the cuvette (commonly 1 cm) and c represents the particles concentration.

2.3.2. Surface Potential

Surface potential was measured with Zetasizer (Malvern, NanoZS). Samples of AuNR-CTAB, AuNR-(PAA PAH) and AuNR-(PAA PAH GG), dispersed in ultra-pure water, were read three times and surface charge was calculated using the Smoluchowski equation.

2.3.3. Morphological characterization

To confirm particles rod-shape and the GG coating, transmission electron microscopy (TEM) and scanning electron microscopy (SEM) analysis were performed. Samples were prepared by placing a drop of each type of particles solution above a copper grid and let it dry completely, under a light source. TEM images were acquired using Jeol JEM 1400 and performed at IBMC-INEB, Porto.

SEM samples preparation: samples were dried at approximately 50ºC, either on glass watch or on a mica substrate. The samples dried on glass watch were then glued on carbon tape. Images were taken using a NanoSEM – FEI Nova 200 (FEG/SEM) with an EDAX – Pegasus X4M (EDS/EBSD).

2.4. Particles Stability

2.4.1. Ionic Strength

Stability under different electrolytic concentrations was evaluated by addition of a NaCl solution to AuNR-CTAB, AuNR-(PAA PAH) and AuNR-(PAA PAH GG) particles. Fixed quantities of 2M NaCl were added to 2 mL solutions of each particles type, in order to have the desired final salt concentrations of 1 mM, 5 mM, 10 mM, 20 mM, 50 mM, 0.1 M and 0.5 M. Solutions were properly mixed and left overnight at room temperature. UV-Vis spectra were acquired 24 hours after salt addition.

2.4.2. pH

In order to evaluate particles stability at different pH comprised between 4 and 10, fixed amounts of hydrochloric acid (HCl), for pH below 6, or sodium hydroxide (NaOH), for pH above 6, were added to 2 mL solutions of particles. Solutions were mixed and left overnight at room temperature. UV-Vis spectra were acquired 24 hours after pH modifications.

2.5. Dexamethasone Incorporation

Dexamethasone-loaded nanoparticles were prepared by mixing AuNR coated with PAA and PAH with a dexamethasone solution (6.66 nM, Sigma-Aldrich) for 3 hours, at room temperature in the dark. Then the solution was directly mixed with a GG solution (0.5% w/v), at 90ºC under vigorous stirring for 5 minutes. This mixture was cooled down until room temperature and stirred overnight, in the dark. GG excess was removed by centrifugation.

2.5.1. Fourier Transform Infrared Spectroscopy (FTIR)

In order to detect surface changes motivated by dexamethasone presence, FTIR spectra were recorded on an IR-Prestige-21 (Shimadzu, Japan) controlled by IRsolution software. Particles solutions were dried at 45ºC during overnight, and then crushed with potassium bromide (Sigma-Aldrich) to prepare a tablet. Spectra were taken in the range 500-4500 cm^{-1}.

2.6. *In vitro* studies

2.6.1. Cell culture

SaOS-2 cells (Sarcoma osteogenic) were cultured in Dulbecco's modified Eagle's medium low glucose (Sigma-Aldrich) supplemented with 10% fetal bovine serum (Alfagene) and 1% antibiotic-antimycotic (Alfagene). Cells were grown until confluence at 37ºC and 5% CO_2 atmosphere, with changing of media every three days. Rabbit adipose derived stem cells (ASC) were isolated using the group well-established protocols and culture in α-MEM cell culture media.

2.6.2. Cell viability

Assessment of the potential effect of AuNR on cell viability was performed using a standard 3-(4,5-dimethylthiazol-2-yl)-5(3-carboxymethoxyphenyl)-2(4-sulfofenyl)-2H-tetrazolium (MTS) viability test. All materials were processed under sterile conditions. Particles sterilization was achieved by passing the different solutions through a 0.22 µm filter.

The MTS viability test on SaOS-2 [96] was performed after contact of cells with different types of nanoparticles: AuNR-CTAB, AuNR-(PAA PAH) and AuNR-(PAA PAH GG).

SaOS-2 cells were grown as monolayers as described above. After several passages, confluent cells were detached from the flasks using TrypLE™ Express Enzyme (Life Technologies) and a diluted suspension was centrifuged at 1200 rpm for 5 minutes. SaOS-2 cells were seeded in each well of a 24-well TCPS plate (three replicates per sample) at a

density of 25 x 10^3 cells/well and cultured for 24 hours at 37ºC in a 5% CO_2 atmosphere. Then, cells were incubated with 200 µL of each type of nanoparticles, making up a final concentration of 0.05 nM/well. The medium was changed every three days, followed by an addition of new particles. Cells without particles were used as a control. The MTS test was performed after 3, 6 and 9 hours and 1, 2, 3, 7 and 14 days of culture at 37ºC and 5% CO_2 atmosphere. Culture medium was removed and cells were washed twice with phosphate buffered saline solution (PBS) at pH 7.4. Subsequently, 350 mL of a mixture containing serum-free culture medium without Phenol Red and MTS (CellTiter W 96 AQueous One Solution Cell Proliferation Assay kit; Promega) at a ratio of 5:1 was added to each well. Optical density (OD) was measured at 490 nm using a microplate reader (Synergy HT, Biotek) after 3 hours incubation at 37ºC and 5% CO_2 atmosphere. The percentage of cell viability was calculated by normalization with the mean OD value obtained for the control. All tests were performed in triplicate (n= 9).

Similar *in vitro* cytotoxicity studies were performed using rabbit ASC. The cells were incubated with AuNR-(PAA PAH GG) and cell viability was quantified after 1, 7 and 14 days. The procedure was similar as the one for SaOS-2, but 96-well plates were used with a cell density of 4 x 10^3 cells/well. This experiment was performed with n=6.

2.6.3. Nanoparticles Uptake

2.6.3.1. Optical Microscopy

SaOS-2 cells were cultured in the same conditions used for MTS assay, but on the top of TCPS cover slips. Cells were grown during, 3, 6 and 9 hours and 1, 2, 3, 7 and 14 days. After each time point, cell culture medium was removed and cells were washed twice with PBS buffer. Then, cells were fixed with 10% formalin for 15 minutes, at room temperature. After, formalin was removed; cells were washed with PBS and stored in PBS, protected from light at 4ºC, until staining.

Cells were stained with 4,6-Diamidino-2-phenyindole, dilactate (DAPI) and Phalloidin–Tetramethylrhodamine B isothiocyanate (phalloidin – TRITC) in order to mark nuclei and the cytoskeleton, respectively. To do so, cells were permeabilized with a 0.2% solution of Triton™ X-100 (Sigma-Aldrich) for 5 minutes. Then, cells were washed twice with PBS and a solution of phalloidin – TRITC (Sigma – Aldrich) diluted 1:200 in PBS was added. After 45 minutes at room temperature, the dye was removed and cells were washed again, with PBS. At last, cells were incubated at room temperature with a solution of DAPI (Sigma – Aldrich) diluted in PBS (1:1000), for 5 minutes. After another washing step, cover slips were mounted with Vectashield (Vector Laboratories) on microscope lamellae, and sealed with nail polish. Samples were finally analysed by fluorescence microscopy and dark field microscopy. The dark-field and fluorescence images were acquired in fast sequence with a wide-field inverted fluorescence microscope (Nikon, model Ti-E). Dark-field imaging was enabled through a dedicated dry dark-field condenser providing an illumination aperture between 0.8 and 0.95 enabling imaging with a 40x objective with collection numeric aperture of 0.75 (CFI Plan Fluor, Nikon). Fluorescence excitation is provided by a high performance broadband Xenon

light source integrated with a fast excitation filter wheel coupled via a liquid light guide to the microscope.

2.6.3.2. Transmission Electron Microscopy

Rabbit ASC were seeded in 24-well culturing plates using a density of 25 x 10^3 cells/well. After an overnight, AuNR-(PAA PAH GG) were added to culture medium at a concentration of 0.05 nM/well. During 14 days, the medium was changed every three days, followed by a particles supplement. After the treatment, cells were detached and centrifuged and the cell pellet was washed with PBS. Cells were centrifuged and the new pellet was fixed with 2.5% glutaraldehyde. The Histology and Electron Microscopy Service of IBMC-INEB Porto performed post-fixation work. For SaOS-2, IBMC facility performed a post-fixation work on cells fixed as described for optical microscopy.

2.7. Statistical analysis and Software

Cell viability data was averaged and mean ± standard deviation was plotted. The data was statistically compared by a "Two-Away ANOVA" analysis and complemented with Bonferroni post-tests. In all statistical evaluations, $p<0.05$ was considered as statistically significant. Statistical analysis was performed using GraphPad Prism 6 software. UV-Vis data were treated and analysed using the Origin9 software (OriginLab).

- *This page was intentionally left blank.* -

Chapter 3

Results

3.1. Synthesis and Characterization of Gold Nanorods

The UV-Vis spectrum (Figure 9, black line) exhibits a typical AuNR sample stabilized with CTAB in water, where the peaks at 510 nm and 820 nm correspond to the transverse and longitudinal resonances, respectively. With the goal of removing the excess of CTAB, which is cytotoxic for cells, the AuNR were washed three times and re-dispersed in purified water. Figure 9 represents the UV-Vis spectra of as-prepared AuNR (red line) and purified AuNR (black line). From figure it is possible to observe that after three washing steps, the amount of free CTAB decreases, as noticed by a decrease of absorbance in a range of 200-300 nm. The purified AuNR exhibit a zeta potential of +35.9 ± 1.3 mV, due the positive charge of CTAB.

The TEM and SEM images (Figure 10) of AuNR revealed that the nanorods have an average length of 47 ± 10 nm and 10 ± 2 nm in diameter with an aspect ratio of approximately 4.7.

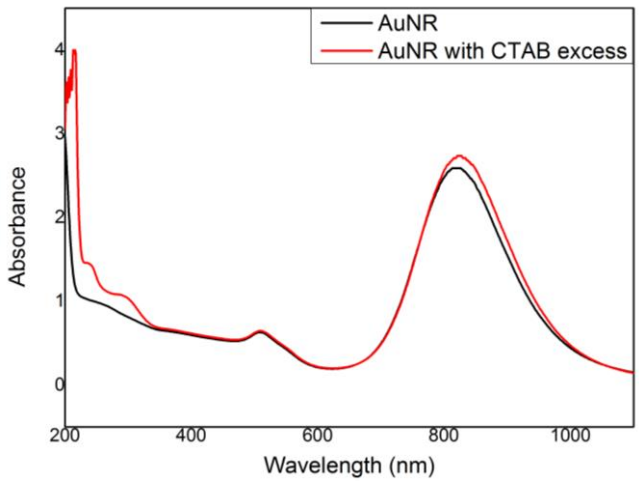

Figure 9 - UV-Vis spectra of AuNR before (black line) and after (red line) the washing step.

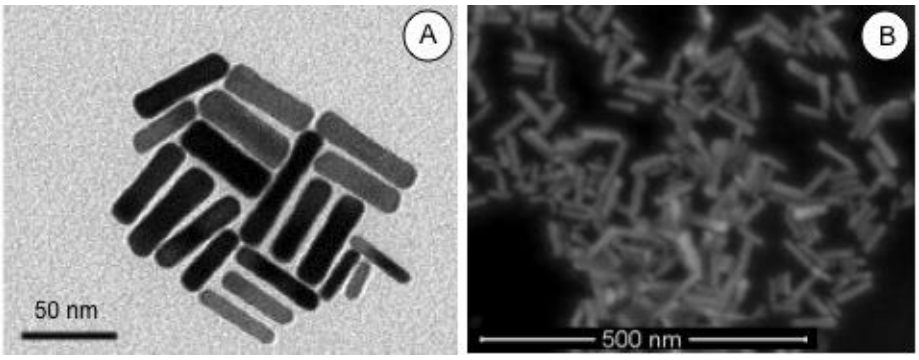

Figure 10 – A: TEM images of AuNR with and 250 000x magnification; B: SEM images of AuNR with 200 000x magnification.

3.2. Surface Functionalization

In the aim of masking and displacing the CTAB layer to make AuNR more biocompatible and stable, the particles were capped with two layers of polyelectrolytes following the LbL method. Based on electrostatic interactions between the different compounds, the negative poly(acrylic acid) (PAA) and a positive poly(allylamine hydrochloride) (PAH), were alternatively adsorbed on the AuNR-CTAB surface, as represented in Figure 11.

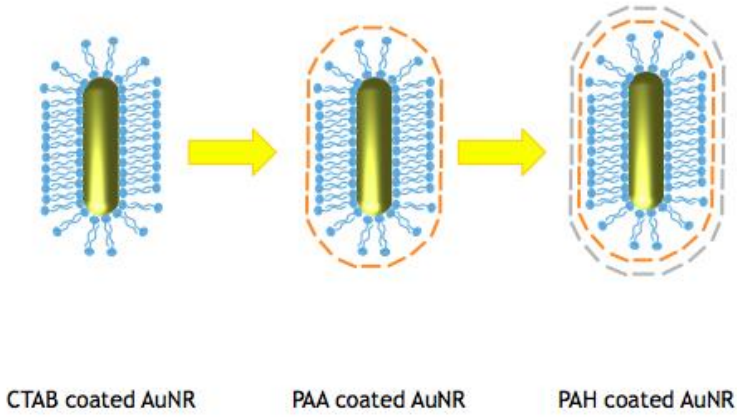

Figure 11 – Schematic representation of layer-by-layer approach for AuNR modification.

The successful multilayer coating was confirmed via zeta potential measurements at each step of the process since the charge of the particles were in agreement with the net charge of each compounds. The AuNR are positively charged with ζ = +35.9 ± 1.3 mV, due to the presence of cationic CTAB bilayer on the surface. After the reaction with anionic PAA, the zeta potential was negative, ζ = -52.4 ± 3.9 mV, changing to a positive value of ζ = +43.5 ± 2.8 mV after the functionalization with cationic PAH.

Figure 12-A exhibits the UV-Vis spectra before and after the polyelectrolyte functionalization. For clarification, it is worth mention that normalization of absorption spectra at the maximum of the longitudinal resonance has been performed. The exchange of capping agent, by successive deposition of PAA and PAH, does not lead to aggregation, since

a narrow LPB is observed in each UV-Vis spectrum. Figure 12-B shows a representative TEM image of AuNR-(PAA PAH). Due to the small dimensions of polyelectrolyte coating, it is not distinguishable on TEM images.

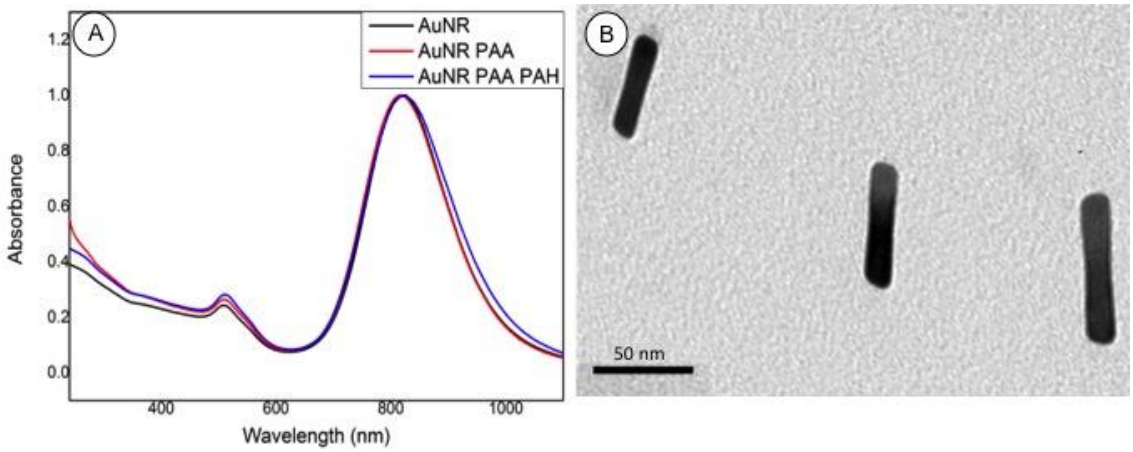

Figure 12 - A: UV-Vis spectra of AuNR, AuNR coated with PAA and AuNR-(PAA PAH); B: TEM image of AuNR-(PAA PAH) with a magnification of 250 000X.

3.3. Gellan Gum Coating

Finally, the AuNR-(PAA PAH) were coated with gellan gum (GG) as schematically represented in Figure 13. To confirm the successfully adsorption of GG on particles surface, AuNR-(PAA PAH GG) were characterised by UV-Vis spectrometry, zeta potential and electron microscopy analyses.

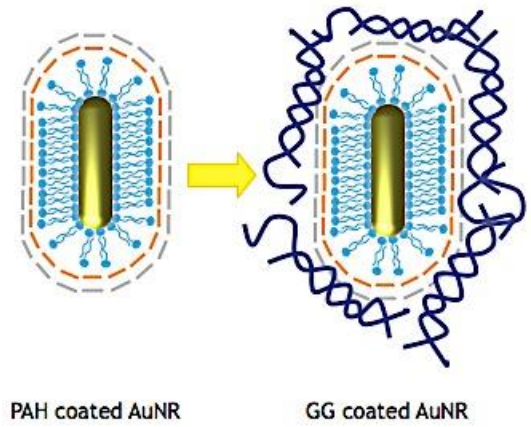

Figure 13 – Schematic representation of AuNR-(PAA PAH) modification with GG.

The UV-Visible spectra of AuNR-(PAA PAH) and AuNR-(PAA PAH GG) are shown in Figure 14-A. After GG coating, the LPB underwent a red-shift of 8 nm, which is a result of the change in the surrounding environment of particles. Moreover, the presence of GG is confirmed via a band located at 260 nm. As shown in Figure 14-B, GG present a band at this wavelength. Zeta potential measurements also have confirmed the modification of particles

surface charge, caused by the incorporation of negatively charged GG. Therefore, after this coating, particles acquired a negative charge of -32.8 ± 4.9 mV.

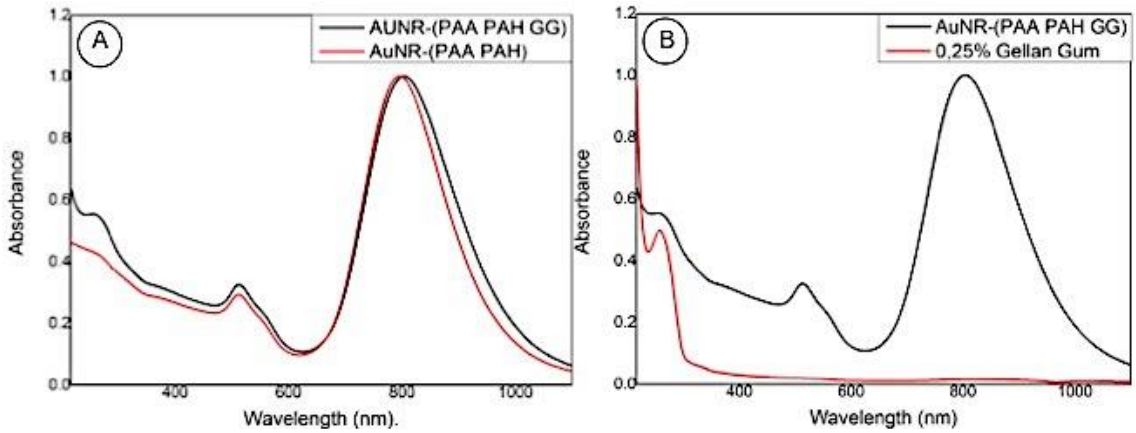

Figure 14 – A: UV-Vis spectra of AuNR-(PAA PAH) (red line) and AuNR-(PAA PAH GG) (black line); B: UV-Vis spectra of AuNR-(PAA PAH GG) (black line) comparing to the spectrum of a 0.25% w/v GG solution (red line).

TEM and SEM analysis were performed to confirm the formation of a GG shell around AuNR. TEM images (Figure 15-A and Figure 15-B) clearly show, contrarily to the polyelectrolyte-coated AuNR (Figure 12-B), the presence of a GG shell around individual AuNR. Shell thickness was measured as 6.8 ± 1.5 nm. SEM was used to assess the surface morphology of the hybrid nanoparticles. However, the resolution of SEM equipment used on this study was not sufficient to fulfil this aim (Figure 15-C). Backscattered electrons analysis (Figure 15-D), which can discriminate different compounds based on their atomic number, indicates that gold is the core of particles.

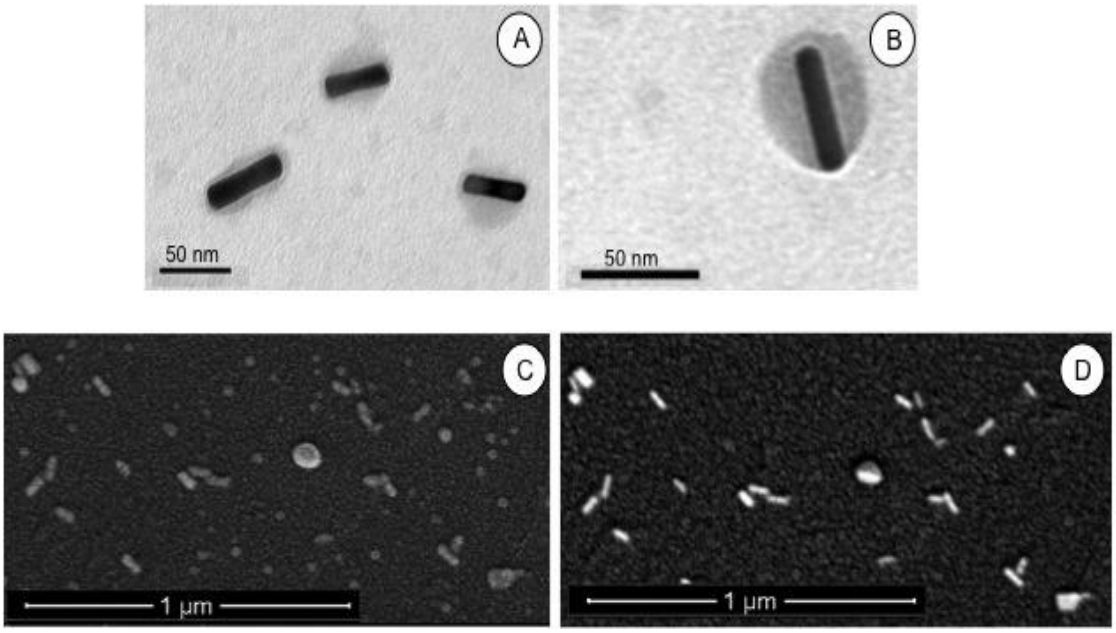

Figure 15 – A: TEM image of AUNR-(PAA PAH GG) particles with 150 000X magnification; B: TEM image of AuNR-(PAA PAH GG) with 250 000X magnification; C: SEM image of AuNR-(PAA PAH GG); D: Backscatter electron analysis of AuNR-(PAA PAH GG).

3.4. Stability Studies

Particles behaviour on different settings was determined based on their UV-Vis spectrum, since LPB is very sensitive to particle aggregations.

Ionic Strength:

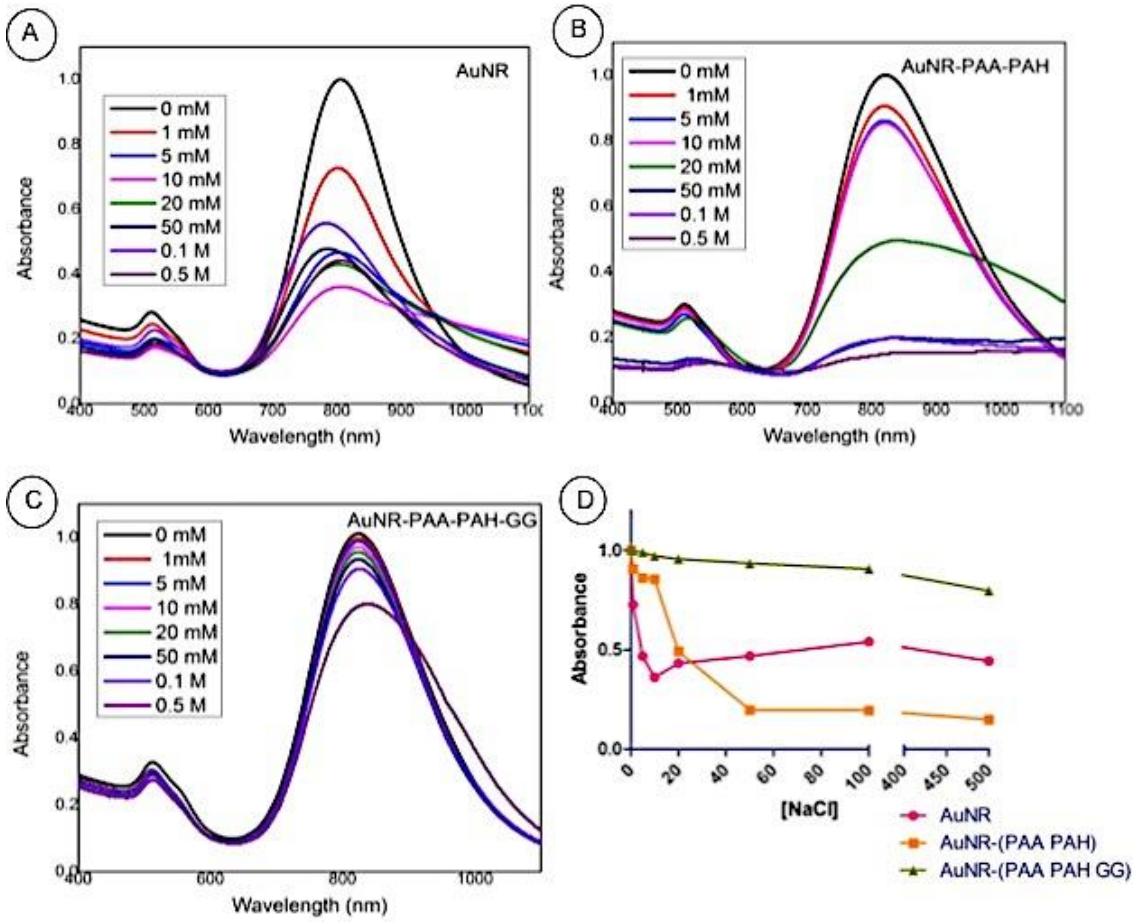

Figure 16 – UV-Vis spectrometry analysis of ionic strength influence on particles stability. Defined concentrations of NaCl were added to solutions of (A) AuNR-CTAB, (B) AuNR-(PAA PAH) and (C) AuNR-(PAA PAH GG) and the respective UV-Vis spectra were acquired after an overnight; (D) Absorbance as a function of salt concentration. For each type of particle, absorbance was measured at maximum wavelength found on particles without salt.

The ionic strength was varied by addition of different volume of a solution of 2 M of NaCl. The final salt concentration in the AuNR modified and unmodified solutions were in a range of concentrations from 1 mM to 0.5 M.

As-prepared AuNR were shown to be the most susceptible to variations of salt concentration (Figure 16-A). Indeed, as soon as the salt concentration increased to 1 mM, a significant change of the longitudinal plasmon band, intensity decrease and widening of the band, is observed, resulting from the gold nanoparticles aggregation. Interestingly, for AuNR-CTAB a maximum state of aggregation was noticed for a concentration of 10 mM, corresponding to a lower absorbance value (Figure 16-D), but it was partially reversed with higher salt concentrations. AuNR-(PAA PAH) appeared to be more stable than AuNR-CTAB, but changes on UV-Vis spectra were also detected (Figure 16-B). When NaCl concentration

reached 20 mM, LPB became wider and the drop of intensity is clearly noticed (Figure 16-D). Those effects became more and more evident with higher concentrations, showing that particles aggregate under these conditions. The presence of GG at NP surface improved the ionic strength stability up to 0.1 M (Figure 16-C), since the LPB remained basically at the same position with a slight absorbance decrease (Figure 16-D). At 0.5 M, the particles start to aggregate, highlighted by a decrease of absorbance amplitude, broadness of LPB and a red-shift of approximately 13 nm.

pH effect:

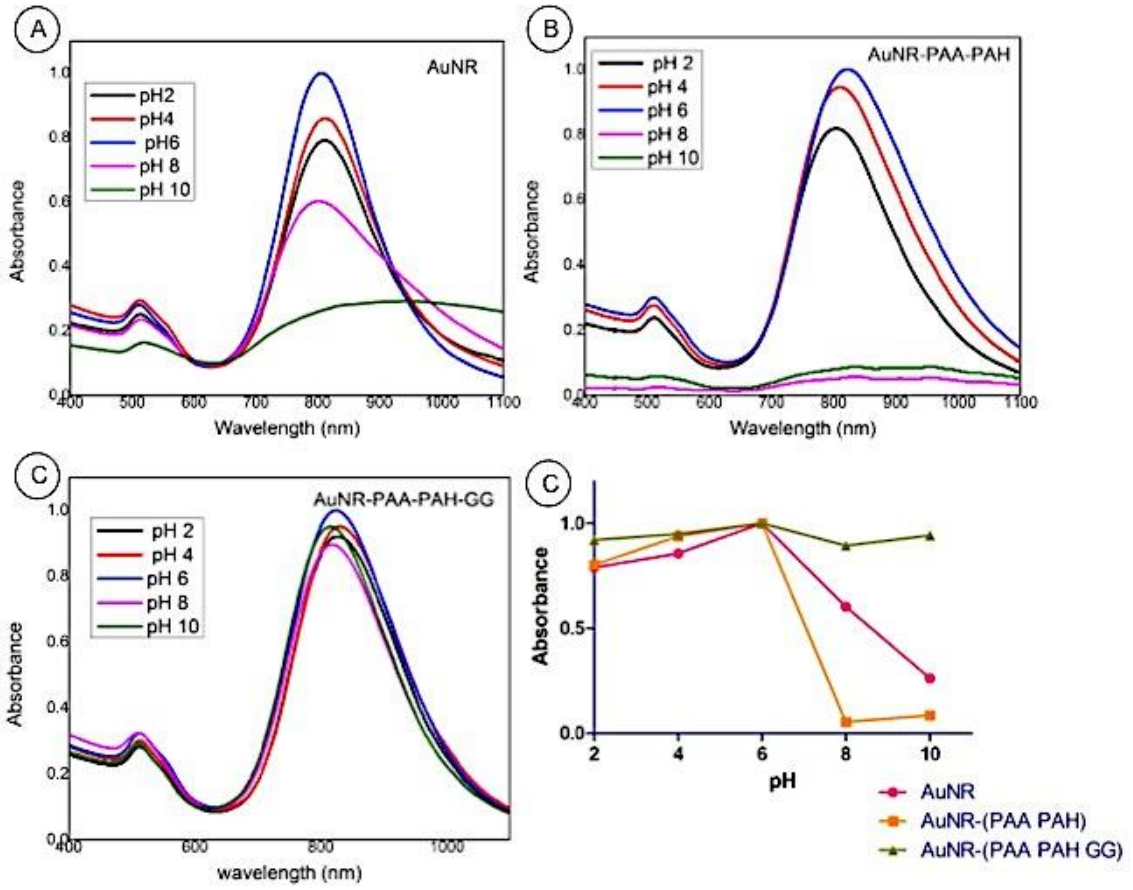

Figure 17 - UV-Vis spectrometry analysis of pH influence on particles stability. Defined concentrations of HCl and NaOH were added to solutions of (A) AuNR-CTAB, (B) AuNR-(PAA PAH) and (C) AuNR-(PAA PAH GG) in order to get acidic and basic conditions, respectively. The respective UV-Vis spectra were acquired after an overnight; (D) Absorbance as a function of pH. For each type of particle, absorbance was measured at maximum wavelength found on particles at pH=6.

The pH was modified by addition of hydrochloric acid (HCl) for pH below 6 and by addition of sodium hydroxide (NaOH) for pH above 6.

The improved stability of AuNR with GG was also noticed when pH was changed. Both AuNR-CTAB and AuNR-(PAA PAH) were susceptible to basic pH (Figure 17-A and B). In both cases, the LPB became wider and absorbance drop occurs, compared to the spectrum at pH 6. The pH effect was more discernible in AuNR-(PAA PAH) (Figure 17-B, green and pink line), where LPB almost disappeared. Acidic pH did not change the shape of LPB, but a shift on its

position and decrease on its intensity was noticed (Figure 17-D, pink and yellow line). On AuNR-CTAB, acidic pH led to a decrease in LPB intensity followed by a red-shift of 5 nm (Figure 17-A, black and red lines). On its turn, the same conditions, caused a blue-shift on LPB of AuNR-(PAA PAH) of 11 nm and 20nm at pH=4 and pH=2, respectively. However, the UV-Vis spectra of AuNR-GG (Figure 17-C) show narrow LPB for the different pH, highlighting that the presence of GG lead to improve AuNR stability. Although no obvious change by UV-Vis was observed (Figure 17-D, green line), at acidic pH we clearly observed by eye that the particles start to flocculate.

3.5. In vitro Studies

3.5.1. Cell viability

For each surface modification step, cytotoxic assays were performed in order to evaluate the biocompatibility of AuNR-CTAB, AuNR-(PAA PAH) and AuNR-(PAA PAH GG). Firstly, two different concentrations of 0.04 nM and 0.08 nM of particles per well were tested, in order to evaluate possible cytotoxicity over SaOS-2 cells. An MTS assay was performed to determine cell viability after 24 hours of incubation in presence of particles. The obtained absorbance values were normalized by the control sample (i.e. without presence of particles). Then, graph represents the percentage of viability comparing to control.

Figure 18 represents the cell viability results obtained for both concentrations. Whereas it is clearly observed that AuNR-CTAB are cytotoxic, for 0.04 nM and 0.08 nM of AuNR-(PAA PAH) and AuNR-(PAA PAH) it was observed no deleterious effect on the SaOS-2 cells viability. No difference was noticed between the two conditions for modified particles and the control. Considering the data obtained from the *in vitro* studies and other values found on literature [26, 33], the chosen concentration for further studies was 0.05 nM/well.

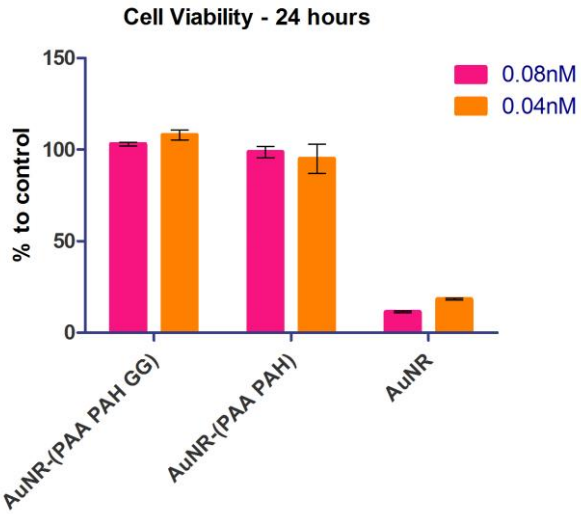

Figure 18 – Cell viability of SaOS-2 after 24 hours, with different types of particles at 0.08 nm and 0.04 nM.

Cell viability was then assessed culturing SaOS-2 cells with different types of particles, for different time points: 3 hours, 6 hours, 9 hours, 24 hours, 72 hours, 7 days and 14 days. As it

is shown in Figure 19, cell viability in presence of AuNR-CTAB decreased along the 14 days of study. After 6 hours of incubation, cell viability start to decrease comparatively to control, reaching only 81% of the viability observed in control cells. In the end of the study period, cell viability was only 5%, confirming the deleterious effect of CTAB on SaOS-2 viability. The difference on cell viability between control and cell incubated with particles start to be significant after 6 hours, with $p<0.01$. From 9 hours up to 14 days, the difference was also significant but with a $p<0.001$. On the other hand, after 14 days of incubation, the presence of AuNR-(PAA PAH) and AuNR-(PAA PAH GG) did not affect cell viability significantly, and cell viability was always superior to 93%.

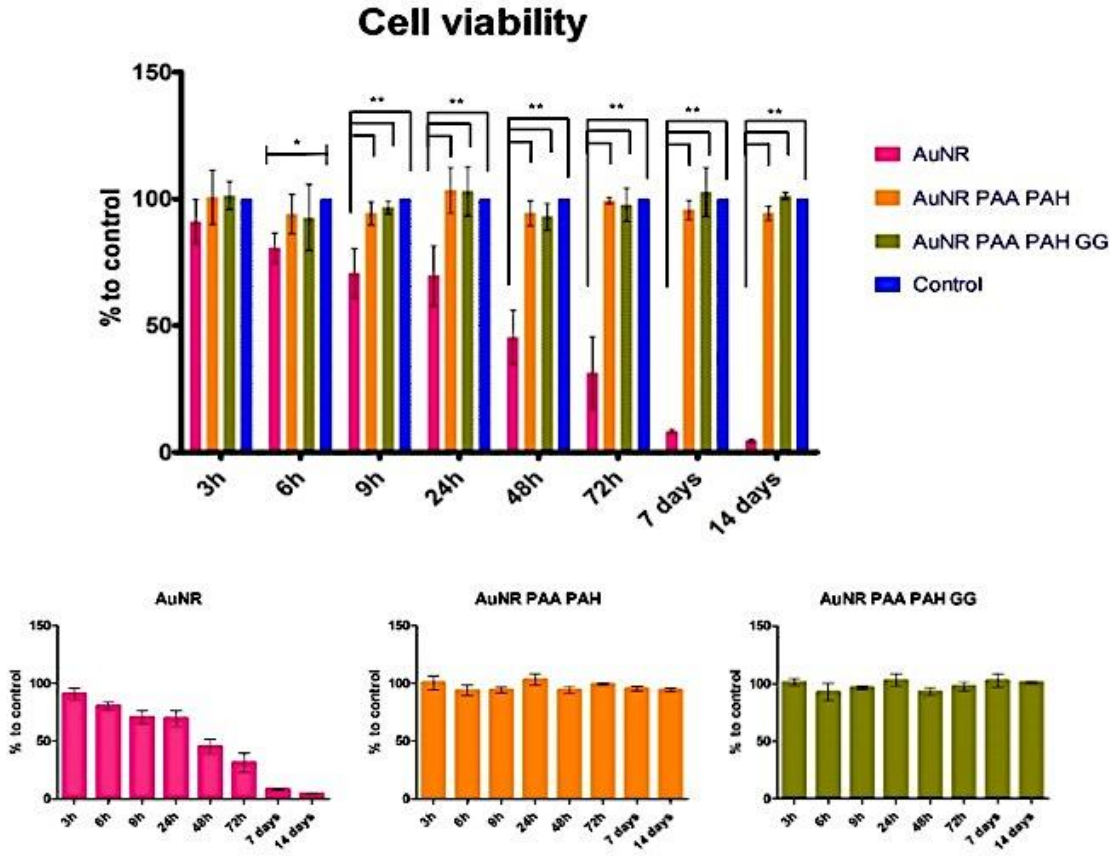

Figure 19 - Cell viability of SaOS-2 cell line cultured with AuNR, AuNR-(PAA PAH) and AuNR-(PAA PAH GG) for 14 days, comparing to control; Upper panel it is a general view of all data. The inferior one represents the same data but organized by particles type. From left to right: cell viability when incubated with AuNR, AuNR-(PAA PAH) and AuNR-(PAA PAH GG). Results expressed as an average ± standard deviation. (n=9, * $p<0.01$; ** $p<0.001$).

Considering that AuNP cytotoxicity varies between different cell types, cell viability was also performed on rabbit adipose derived stem cells. Cell viability was assessed after 1, 7 and 14 days of incubation with AuNR-(PAA PAH GG) (Figure 20). Surprisingly, cell viability was higher in all the tested time-points, confirming the non-toxic nature of AuNR-(PAA PAH GG).

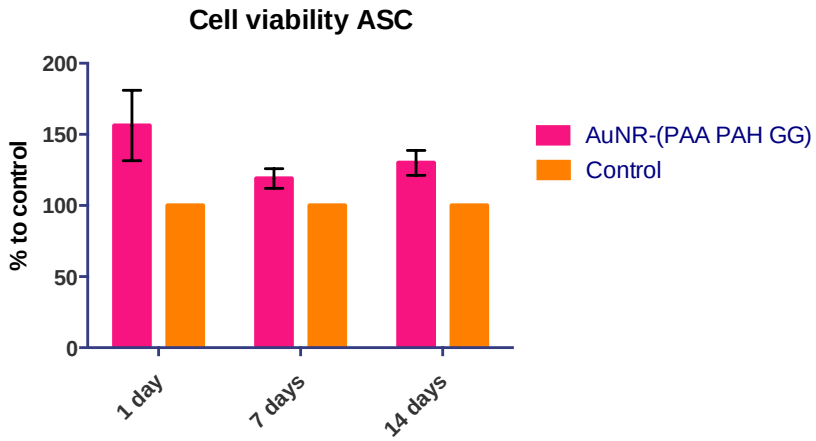

Figure 20 - Cell Viability of ASC cultured with AuNR-(PAA PAH GG) for 1, 7 and 14 days, comparing to cell viability of ASC without particles. Results expressed as an average ± standard deviation. (n=6).

3.5.2. Internalization of AuNR

Taking advantage of optical properties of AuNP, particles internalization was analysed by fluorescence microscopy with dark-field. The nuclei were stained with DAPI and the cytoskeleton with Phalloidin-TRITC, to allow the observation of cell morphology under fluorescence microscopy, after incubation with the AuNR-(PAA PAH GG). Next, scattering and fluorescence images were simultaneously acquired with dark-field microscopy and fluorescence microscopy (Figure 21). The red parts show the cytoskeleton and the blue parts the nuclei (Figure 21-A and Figure 21-C). By its turn, the bright spots in dark-field images (Figure 21-B and Figure 21-D) result of the light scattering of AuNR.

Analysing the dark-field images, one can see that no brightness is noticed in control samples (Figure 21-B). However, in samples incubated with AuNR-(PAA PAH GG) these bright spots were found, meaning that modified AuNR were internalized by SaOS-2 cells after 48 hours (Figure 21-D). From fluorescence images, it can be seen that there is a small difference in cell morphology between the two conditions, control (Figure 21-A) and AuNR-(PAA PAH GG) (Figure 21-C). Although spread cells were found in both conditions, comparing to untreated cells, the number of round shape cells appeared to be higher when cells were cultured with the particles.

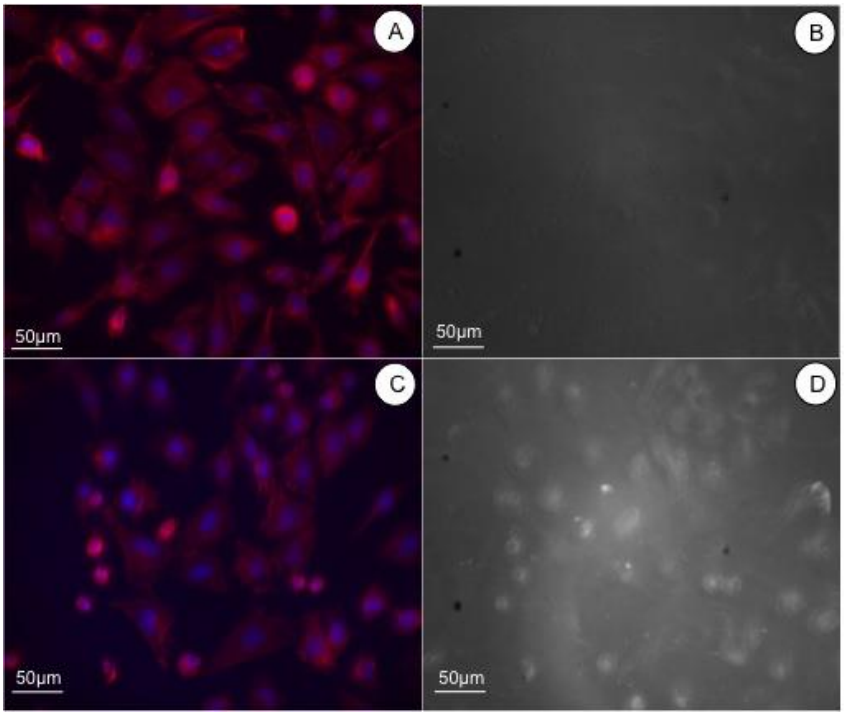

Figure 21 - Fluorescence microscopy of SaOS-2 incubated without particles (A) and with AuNR-(PAA PAH GG) (C) for 48 hours. Red areas represent the cytoskeleton stained by Texas Red – X phalloidin and blue areas the nuclei, stained with DAPI; dark filed microscopy of the same samples (B) and (D) respectively.

AuNR-(PAA PAH GG) internalization after 14 days of culturing was also evaluated by TEM, both on SaOS-2 and rabbit ASC. Internalization was observed in both conditions, as shown in Figure 22 and Figure 23, respectively. Particles were localised inside cytoplasmic vesicles, forming aggregates. Nevertheless, it is important to notice that the vesicles observed were different. While in SaOS-2 particles were found mostly in multi-layered vesicles, particles were surrounded by one-layered vesicles when uptaken by ASC. Thence, intracellular traffic after AuNR-(PAA PAH GG) internalization may differ among the tested cells.

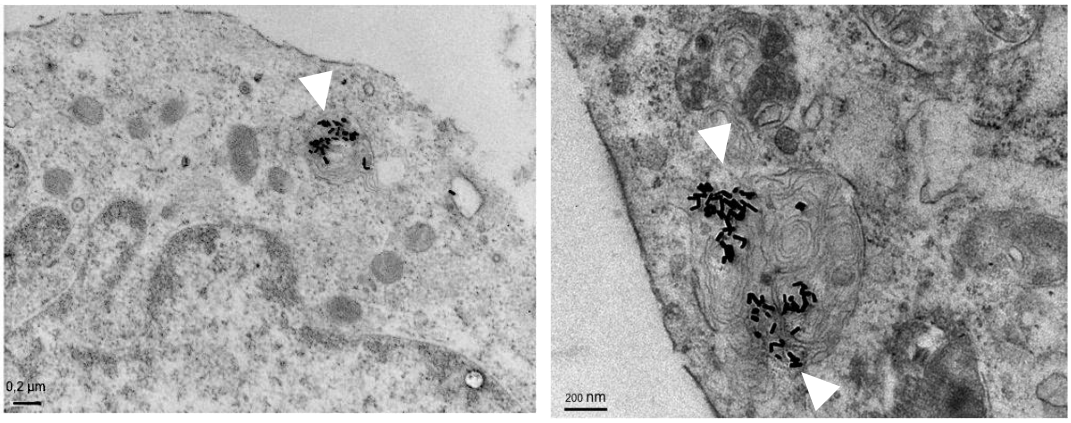

Figure 22 - TEM images of SaOS-2 after 14 days of incubation with AuNR-(PAA PAH GG) at 0.05 nM. AuNR-(PAA PAH GG) aggregated within cytoplasmic vesicles, shown with arrows. Magnification of 40 000X (left) and 60 000X (right).

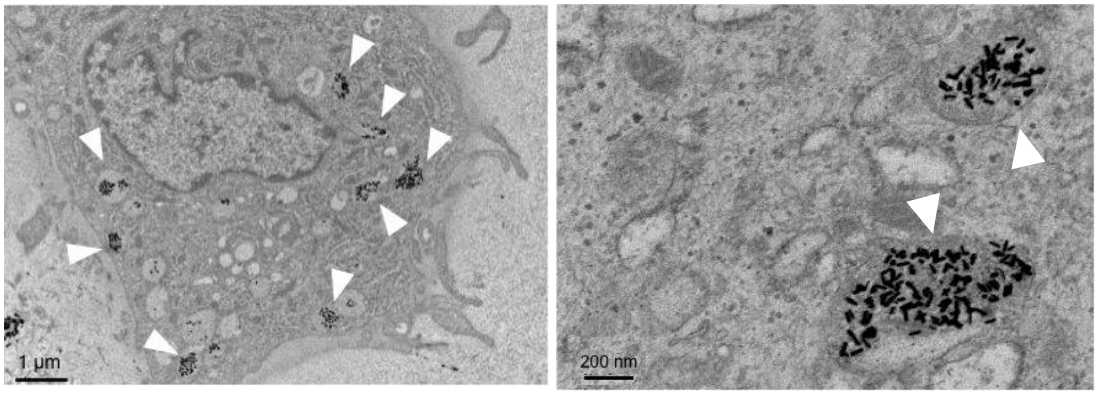

Figure 23 - TEM images of rabbit ASC after 14 days of incubation with AuNR-(PAA PAH GG) at 0.05 nM. AuNR-(PAA PAH GG) aggregated within cytoplasmic vesicles, shown with arrows. Magnification of 1 200X (left) and 50 000X (right).

3.6. Incorporation of Dexamethasone

The incorporation of dexamethasone was done right after the PAH coating, by adding particles to a dexamethasone solution. These particles were then mixed with a GG solution with final concentration of 0.25% w/v, in order to obtain AuNR-(PAA PAH GG) loaded with dexamethasone. As before, modified particles were washed by centrifugation.

The aforementioned method was performed using AuNR-(PAA PAH) and AuNR-(PAA PAH GG). However, the first ones aggregated after the first centrifugation cycle, precluding their use in further experiments. Figure 24-A shows the UV-Vis spectra of AuNR-(PAA PAH) with dexamethasone before the washing and after the first two steps of the cycle. Since particle aggregation was noticed during the lower speeds, the cycle was not completed.

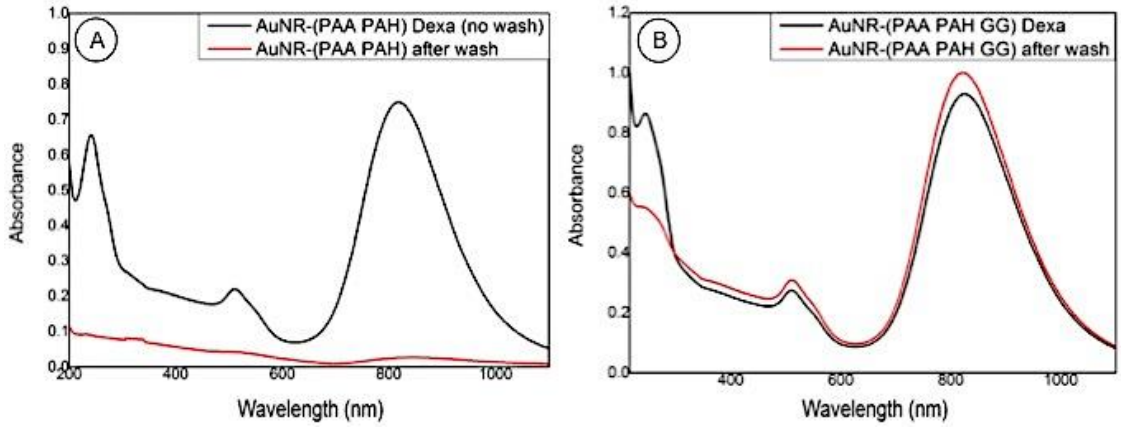

Figure 24 – UV-Vis spectra of AuNR-(PAA PAH) (A) and AuNR-(PAA PAH GG) (B) after loading with dexamethasone. In both graphs, the black line is the UV-Vis spectra of particles before washing; while the red line represents the UV-Vis spectra of particles after one wash cycle.

As it is shown in Figure 24-B, the UV-Vis spectrum of particles that were covered with a GG layer did not change in a substantial way during the washing cycle. Hence, covering particles with a GG layer led to particles with more stability, which did not aggregate right after centrifugation.

Although it was possible to evaluate particles stability after the drug loading process, its efficiency was not as straightforward. Electronic absorption spectroscopy was not suitable, since UV-Vis spectra of GG and Dexa overlap in the wavelengths between 226 nm and 281 nm, as it is shown in Figure 25.

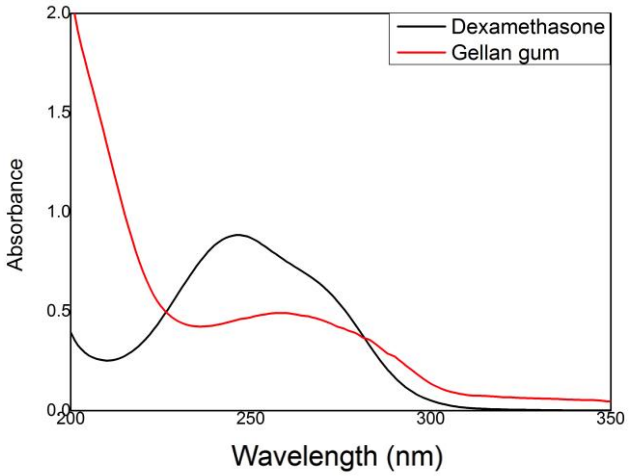

Figure 25 – UV-Vis spectra of Dexamethasone (black line) and Gellan Gum (red line).

FTIR spectroscopy was also carried out in order to assess on dexamethasone loading. In addition to the partial overlap of AuNR-(PAA PAH GG) spectra with the one corresponding to dexamethasone, drug concentration inside particles may be below the detection limits of the technique (Figure 26).

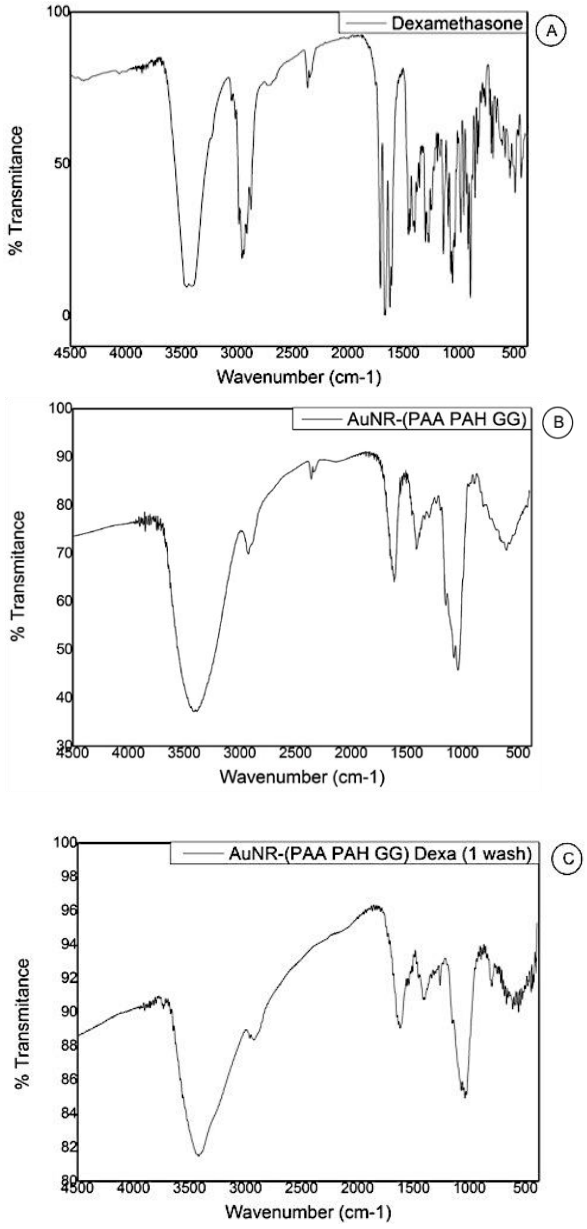

Figure 26 - FTIR spectra of (A) dexamethasone; (B) AuNR-(PAA PAH GG); (C) dexamethasone loaded AuNR-(PAA PAH GG).

- *This page was intentionally left blank.* -

Chapter 4

Discussion

Due to their unique and remarkable properties, gold nanoparticles caught attention of researchers in diverse areas. As aforementioned, biocompatibility, ease of synthesis, chemical inertness and their optical and photothermal properties are some of the key features that made them so interesting to the scientific community. As alternative to spherical nanoparticles, AuNR, an anisotropic shape of AuNP, are commonly used for biomedical purposes [14]. Additionally to AuNP advantages, AuNR can be tuned in size in order to absorb in the NIR region of the spectra. Since tissues do not absorb in this region of the spectra, AuNR can be used both for imaging purposes, for controlled drug release approaches, with NIR triggered release, and for hyperthermia therapies.

In the present work, it has been reported the development of a novel method for AuNR functionalization, taking advantage of stabilizing and biocompatible properties of gellan gum. Firstly, well-dispersed AuNR were successfully synthesized by a seed-mediated growth method [25], using CTAB as surface passivant. To prepare AuNR with a LPB located above 800 nm, hydrochloric acid was added to the growth solution. Indeed, it has been observed that the synthesis of AuNR in acidic pH lead to the formation of longer particles, resulting in a shift of the LPB in the NIR [97].

The as-prepared AuNR presented in their UV-Vis spectrum two bands, located at 510 nm and 820 nm, corresponding to the transverse and longitudinal plasmon, respectively. TEM images revealed homogeneous AuNR with an average length of 47 ± 10 nm and an aspect ratio of approximately 4.7.

The preparation of biocompatible nanomaterials is essential for their use in biomedical applications. However, the AuNR synthesis method implies the use of CTAB, which has cytotoxic effects. Even though centrifugation partially removes free CTAB molecules, is still necessary to modify AuNR surface.

AuNR-(PAA PAH GG) were then prepared in two sequential steps. Firstly, the gold nanorods were covered with a thin bilayer of polyelectrolytes to improve their stability and

to mask the CTAB on the AuNR surface. In the process of AuNR synthesis, the CTAB forms a cationic bilayer at the surface of AuNR and generate a positive charge of +35 mV. Therefore, based on the LbL method, alternative layers of opposite charged polyelectrolytes can be adsorbed on the positive AuNR via electrostatic interactions. Herein, polyelectrolyte-modified AuNR were achieved by sequential adsorption of the negatively charged PAA, followed by the adsorption of positively charged PAH. Accordingly, the addition of PAA changes the surface charge from positive to negative values (ζ= -52.4 ± 3.9 mV), and flipped again to positive values after PAH coating (ζ= 43.5 ± 2.8 mV). The UV-Vis spectra of both AuNR-PAA and AuNR-(PAA PAH) remained similar to the AuNR-CTAB one, suggesting that after polyelectrolyte modification the particles remain stable and well-dispersed in purified water. Then, the PAH-modified AuNR were added to a low acyl gellan gum solution. Due to the negative charge (p*K*a=3.1) of GG in purified water, GG may adsorb on the positively charged AuNR-(PAA PAH) via electrostatic interaction. However, dry gellan gum is not miscible in water at room temperature. To allow its dissolution, 0.5% w/v GG in solution need to be previously heated at 90ºC before the addition of the particles [71]. The mixture was then stirred during 5 minutes at 90ºC to allow a good dispersion of the particles within the polysaccharide and then left overnight at room temperature. Upon decreasing the temperature, gellan gum may form a hydrogel-like structure around the particles. Centrifugation steps were then performed to remove the excess of GG, and resulting nanoparticles were characterized by different techniques to confirm the formation of the GG shell on the AuNR surface. By UV-Vis analysis it was possible to observe that the LPB underwent a red-shift, arising probably to a change of the surrounding environment during the adsorption process. Moreover, UV-Vis spectrum of the hybrids exhibits a new band located at 260 nm, attributed to the presence of the GG. The AuNR-(PAA PAH GG) have a negative zeta potential of -32.8 ± 4.9 mV, indicating both the presence of the anionic GG and good stability of the nanoparticles in aqueous solution. Zeta potentials higher than +25 or below -25 mV are considered to be the threshold values for stable colloidal suspensions. Our process of coating has shown the successful preparation of AuNR-(PAA PAH GG) core-shell structure, where individual AuNR are coated by homogeneous GG shell around 7 nm, as revealed by the TEM image. Unfortunately, results from SEM analyses were not conclusive, due to the low resolution of the equipment.

When designing nanoparticles for biomedical applications, stability under different pH and ionic conditions should be considered. To assess this question, we measured and compared the UV-Vis spectra of AuNR-CTAB, AuNR-(PAA PAH) and AuNR-(PAA PAH GG) when dispersed in a range of pH and electrolytic conditions. Due to sensitivity of LPB to particle aggregation, it is possible to analyse and compare particles stability under different conditions. The aggregation is noticed via shifts, tailing, broadening and decrease of intensity of LPB.

The ionic strength was evaluated by addition of a solution of NaCl in a range of concentration from 1 mM to 0.5 M. At low salt concentration, AuNR-CTAB have tendency to easily aggregate. Interestingly, one expected to observe a more obvious aggregate state for higher ionic strength, but the absorbance amplitude of LPB increases and the width of the LPB decreased, suggesting that particles are more stable. This results have already been observed under other conditions [98, 99] and explained as following: at low salt concentration, the Cl^- anions bind electrostatically to the positively charged AuNR-CTAB. As a

result, particles experience a charge screening of the electrostatic repulsion, which leads to their aggregation. At higher concentrations of salt, Cl^- concentration is sufficient to form a second electronic layer, minimizing the aggregation of AuNR-CTAB.

AuNR-(PAA PAH) has shown a superior stability than AuNR-CTAB for low ionic strength. Whereas, AuNR-CTAB aggregate from 1 mM, the polyelectrolyte-modified nanoparticles remained stable up to 20 mM and then underwent a progressive aggregation as the ionic strength increases.

Gellan gum heteropolysaccharide has shown to improve the stability of the AuNR in a wider range of salt concentration, from 1 mM to 0.1 M. The UV-Vis spectra of all conditions remain similar with a slight intensity decrease as the concentration increase. At 0.5 M, the amplitude decrease and the wideness and red-shift of the LPB are more pronounced, suggesting that the particles get closer to form aggregate.

The other interesting aspect to study is related to particles stability under different pH conditions. Both AuNR-CTAB and AuNR-(PAA PAH) are unstable under basic pH, as noticed by a change of the LPB, whereas AuNR-(PAA PAH GG) kept stable. Moreover, as the pH increase, the aggregation stages were more pronounced for the both positively charged particles, i.e. AuNR-CTAB and AuNR-(PAA PAH). Indeed, by increasing the pH, the molecules adsorbed on the AuNR are deprotonated. PAH exhibit a p*K*a around 8.6 [33]. At pH<p*K*a, the polyelectrolyte is positively charged due to the protonation of the amino group in $-NH_3^+$, resulting to repulsion between particles that maintain a colloidal stability. However, at pH>8.6, the deprotonated amino group $-NH_2$ has no charge, leading to a decrease of charge repulsion between particles. Therefore, aggregation occurs and is more significant as the pH increases. On the other hand, GG exhibits a p*K*a around 3.06 [100]. At pH>3.1, the gellan gum is negative due to the presence of group COO^-. Under basic pH, the negative repulsion promotes nanoparticles stability. However, under acid pH, the particles should have aggregated, involving a change of LPB. The UV-Vis spectra measured at pH 2 and 4 exhibit a narrow LPB suggesting that the particle are dispersed in solution and not aggregate. With eye, we could observe that the particles flocculate. Gellan gum in general is pH-sensitive and in acidic pH it has the tendency to form a gel [75]. Herein, it has been hypothesized that instead to promote aggregation when decreasing the pH, the GG interacts and embedded the particles in a matrix that protect them against aggregation.

Biological environment requires working at pH around 7-8 and high ionic strength. Therefore, the synthesized hybrid materials have shown more promising features than the polyelectrolytes-modified nanoparticles and the AuNR-CTAB, showing the utility to surface coat the particles with a hydrogel layer.

Once confirmed the ability to functionalize nanoparticles with GG and the improvement of the proposed system under conditions close to the ones present in physiological media, it has been also studied how particles can interact with cells, *in vitro*. Recent studies have shown that AuNP may promote osteogenic differentiation in some cell types [91–93]. Following this idea, along with the rational used by Oliveira *et al*. [93] and Monteiro *et al*. [94], it has been attempted to use AuNR-(PAA PAH GG) as drug delivery system to promote osteogenic differentiation of stem cells. Therefore, cell viability and internalization capacity

in two different cell types has been investigated. Firstly, SaOS-2, a human osteoblast-like cell line commonly used for osteoblastic models [101], were used to test the biocompatibility of AuNR-CTAB, AuNR-(PAA PAH) and AuNR-(PAA PAH GG). Then, and considering the final aim of this work, cell viability on rabbit adipose derived stem cells, which have osteogenic differentiation capacity [102], was investigated after incubation with AuNR-(PAA PAH GG) for 1, 7 and 14 days. Cell viability was assessed using an MTS assay. The MTS tetrazolium compound is bio-reduced by cells into a coloured formazan product, that is soluble in tissue culture medium [103]. NADPH or NADH, produced by dehydrogenase enzymes in metabolically active cells, presumably performs such conversion. Then, the quantity of formazan is directly proportional to the number of living cells in culture.

Since literature is not coherent regarding the appropriate concentration of particles [26], two different concentrations of 0.04 and 0.08 nM/well were tested in SaOs-2 cultures. Contrarily to surface modified AuNR, AuNR-CTAB have induced considerable cytotoxicity after 24 hours of incubation. However, no significant differences were noticed in cell viability between the both conditions. Considering other reported data [33], a concentration of particles of 0.05 nM/well was used on cell viability studies.

When incubated with SaOS-2, AuNR-CTAB were found to be highly cytotoxic, with significant differences relative to control after 6 hours of incubation, when cell viability decreased to 81%. Under these conditions, cell viability has continuously decreased and after 14 days of culture reached only 5%. By its turn, cell viability was not affected by the presence of both AuNR-(PAA PAH) and AuNR-(PAA PAH GG), along the 14 days of study. Such results are in accordance with the ones reported by Alkilany *et al.* [33], who associated AuNR cytotoxicity to the free CTAB molecules. Although centrifugation of particles was performed three times, CTAB still remained on AuNR-CTAB solutions. Further centrifugations are not recommended, though, to not compromise particles stability [98]. The obtained results corroborate that over coating the AuNR with polymers substantially reduces particles cytotoxicity, since CTAB molecules are masked and do not directly interact with cell membranes. Regarding cell viability of rabbit ASC, unexpectedly, AuNR-(PAA PAH GG) promoted cell viability as compared to ASC without particles. Nevertheless, it is necessary to repeat once these experiments, in order to obtain statically significant results and confirm this observation.

Due to their small size, nanoparticles are easily uptaken by cells. Previous studies suggested receptor-mediated endocytosis as the mechanism of cellular uptake for biomolecules within the size range of AuNR [33]. This mechanism is based on the recognition of proteins present on the serum-containing media by receptors of cellular membrane. When included in serum-containing media, media proteins, mostly BSA [33], adsorb on particles surface, changing their surface charge to values similar to the media alone. Thus, particles can be recognized by the cellular receptors and consequently be internalized.

Particle internalization was firstly evaluated with fluorescence and dark field microscopy in SaOS-2 incubated with AuNR-(PAA PAH GG) for 48 hours. Due to the optical properties of AuNR, particles could be distinguished as bright spots when analysed by dark field microscopy, allowing their detection without any additional labelling method. After 48 hours of incubation, it was possible to observe such bright areas inside cells, indicating particles

internalization, as shown in Figure 21-D. However, due to equipment constrains it was not possible to acquire images at higher magnification, that would possible allow a more specific localization of particles within cells. Fluorescence microscopy was used to localise and obtain cell morphology, by means of cytoskeleton and nuclei staining. One interesting observation is that samples incubated with particles had more round-shape cells comparing to control. Although cell viability was similar between cells culture with and without particles, it would be interesting to determine and quantify apoptosis at a single cell level. TUNEL technology, which labels DNA strand breaks associated to apoptosis phenomena, could be used to obtain such information. By this way, it would be possible to understand if the observed round-shape is due to programmed cell death or to other cellular response to AuNR-(PAA PAH GG).

To overcome the low magnification of dark field, and gain deeper insights on how particles behave inside cells, cells were analysed by TEM. On SaOS-2, after 14 days of culture, particles were found inside cells, aggregated within multilamellar vesicles, presumably late endosomes. Likewise, on rabbit ASC, particles were also internalized, but were found inside cytoplasmic vesicles with only one membrane. Such difference can possibly be a result of alternative endocytosis routes, which differ within cell types. Thereby, it would be interesting to study how AuNR-(PAA PAH GG) are internalized and understand their intracellular route once inside cells. This could be achieved using a combination of several methods such as flow cytometry, fluorescence and electron microscopy techniques, as reported by Shapero *et al*. [104]. Although Shapero's work was focused on understanding the behaviour of silica nanoparticles in human cells, the multidisciplinary rational can be applied for AuNR-(PAA PAH GG). High-resolution membrane capacitance measurements could also give interesting data regarding this issue [105]. This method is based on the measurement of plasma membrane capacitance fluctuations, which are due to fusion and fission of secretory and other vesicles. The measurements can be performed on a daily basis, which would allow a continuous study of particles-cell interactions.

As mentioned before, one of the great potential of AuNR-(PAA PAH GG) is for intracellular drug delivery. Considering a previous work of our group, that successfully used dendrimers for intracellular delivery of dexamethasone, we tried to apply such rational to our GG-coated AuNR. Therefore, dexamethasone, a glucocorticoid widely used as supplement in osteogenic media, was adsorbed onto particles surface for further delivery inside cells. The incorporation was performed with AuNR-(PAA PAH) and AuNR-(PAA PAH GG) particles, but only GG capped particles remain stable after the washing process, as seen by UV-Vis analysis. Such observation corroborates the improved stability of AuNR-(PAA PAH GG) as compared to AuNR-(PAA PAH) observed before. Unfortunately, it was not possible to confirm the presence of dexamethasone on particles. UV-Vis cannot be used as a detection method since GG and dexamethasone absorb in the same region of the spectra, between 226 and 281 nm. FTIR analysis was also inconclusive, which could be due to a low concentration of dexamethasone on samples. Moreover, GG and dexamethasone spectra are partially overlapped, hindering the possibility of undoubtedly attest dexamethasone presence in particles. Then, further studies are needed to study dexamethasone loading on AuNR-(PAA PAH GG), in future. Possible approaches for further studies can include the utilization of labelled dexamethasone, either with a fluorescent dye [106] or radioactive labelling [107], or through NMR analysis.

- *This page was intentionally left blank.* -

Chapter 5

Conclusions

In summary, herein it has been reported a new method for gold nanorods (AuNR) surface modification, using natural and biocompatible gellan gum (GG).

A layer-by-layer approach was used to firstly modify AuNR, with aspect ratio of 4.7, with polyelectrolytes and then with GG. TEM images have confirmed the formation of a 7 nm GG shell around individual AuNR. UV-Vis analysis and a zeta potential of -32.8 ± 4.9 mV have proved AuNR stability on ultra-pure water at neutral pH. The potential of these particles as a new tool for biomedical purposes was highlighted by their enhanced stability under a range of pH and ionic strengths, which also shows the feasibility of using GG as stabilizing agent.

Likewise, *in vitro* studies have corroborated the possibility of applying GG-coated AuNR on biomedical applications. No cytotoxicity has been found when GG-coated AuNR were incubated with SaOS-2 and rabbit adipose stem cells at a concentration of 0.05 nM/well, up to 14 days of culturing. Due to AuNR optical properties, it was possible to evaluate particles internalization by dark-field microscopy, without any additional label probe. The results indicated that cells are able to uptake the particles, which was also confirmed by TEM. Once inside cells, particles aggregate within cytoplasmic vesicles, behaviour previously reported for other types of gold nanoparticles. Nevertheless, vesicles morphology was not similar between the two cell types, which may be a result of different intracellular traffic routes.

One of the intended applications for the method here reported is intracellular drug delivery of dexamethasone. When compared to polyelectrolyte-coated AuNR, GG-coated AuNR have shown a higher stability after dexamethasone loading step. Although promising, it was not possible to confirm the effective drug loading.

Therefore, further experiments are needed to confirm and optimize the drug delivery potential of GG-coated AuNR. Following the rational previously proved by our group, one of the applications for the proposed surface-coated particles could be stem cell differentiation, namely osteogenic, by intracellular drug delivery of drugs or growth factors. To investigate this hypothesis, further studies would be performed to compare the differentiation extent of cells incubated with dexamethasone loaded GG-coated AuNR and with the standard osteogenic media. In the future, it would be also interesting to combine the drug delivery

potential of these particles with the remarkable optical properties of AuNR. Such multifunctional system would allow not only to deliver drugs on intracellular compartment, but also track cells in real time, without further labelling.

References

[1] P. X. Zhao, N. Li, and D. Astruc, "State of the art in gold nanoparticle synthesis," *Coord. Chem. Rev.*, vol. 257, pp. 638–665, 2013.

[2] N. Khlebtsov, V. Bogatyrev, L. Dykman, B. Khlebtsov, S. Staroverov, A. Shirokov, L. Matora, V. Khanadeev, T. Pylaev, N. Tsyganova, and G. Terentyuk, "Analytical and theranostic applications of gold nanoparticles and multifunctional nanocomposites.," *Theranostics*, vol. 3, pp. 167–80, 2013.

[3] S. Vial, D. Nykypanchuk, K. G. Yager, A. V Tkachenko, and O. Gang, "Linear Mesostructures in DNA-Nanorod Self-assembly," *ACS Nano*, 2013.

[4] X. Y. Zhang YS, Wang Y, Wang L, Wang Y, Cai X, Zhang C, Wang LV, "Labeling Human Mesenchymal Stem Cells with Gold Nanocages for in vitro and in vivo Tracking by Two-photon Microscopy and Photoacoustic Microscopy," *Theranostics*, vol. 3, pp. 532–543, 2013.

[5] R. Guo, L. Zhang, H. Qian, R. Li, X. Jiang, and B. Liu, "Multifunctional Nanocarriers for Cell Imaging , Drug Delivery , and Near-IR Photothermal Therapy," *Langmuir*, vol. 26, no. 20, pp. 5428–5434, 2010.

[6] Y.-C. Yeh, B. Creran, and V. M. Rotello, "Gold nanoparticles: Preparation, properties, and applications in bionanotechnology," *Nanoscale*, vol. 4, pp. 1871–1880, 2012.

[7] S. Vial, D. Nykypanchuk, F. L. Deepak, M. Prado, and O. Gang, "Plasmonic response of DNA-assembled gold nanorods: Effect of DNA linker length, temperature and linker/nanoparticles ratio.," *J. Colloid Interface Sci.*, vol. 433C, pp. 34–42, Jul. 2014.

[8] S. Parveen, R. Misra, and S. K. Sahoo, "Nanoparticles: a boon to drug delivery, therapeutics, diagnostics and imaging.," *Nanomedicine*, vol. 8, no. 2, pp. 147–66, Feb. 2012.

[9] X. Huang, W. Qian, I. H. El-Sayed, and M. A. El-Sayed, "The potential use of the enhanced nonlinear properties of gold nanospheres in photothermal cancer therapy," *Lasers Surg. Med.*, vol. 39, no. 9, pp. 747–753, Oct. 2007.

[10] H. Yuan, C. G. Khoury, C. M. Wilson, G. A. Grant, A. J. Bennett, and T. Vo-Dinh, "In vivo particle tracking and photothermal ablation using plasmon-resonant gold nanostars," *Nanomedicine : nanotechnology, biology, and medicine*, vol. 8, no. 8. Elsevier,, pp. 1355–1363, 01-Nov-2012.

[11] S. Eustis and M. A. El-Sayed, "Why gold nanoparticles are more precious than pretty gold: Noble metal surface plasmon resonance and its enhancement of the radiative and nonradiative properties of nanocrystals of different shapes," *Chem. Soc. Rev.*, vol. 35, no. 3, pp. 209–217, 2006.

[12] F. Toderas, M. Baia, D. Maniu, and S. Astilean, "Tuning the plasmon resonances of gold nanoparticles by controlling their size and shape," *J. Optoelectron. Adv. Mater.*, vol. 10, no. 9, pp. 2282–2284, 2008.

[13] S. Srivastava, B. L. Frankamp, and V. M. Rotello, "Controlled Plasmon Resonance of Gold Nanoparticles Self-Assembled with PAMAM Dendrimers," *Chem. Mater.*, vol. 17, no. 3, pp. 487–490, Jan. 2005.

[14] Z. Zhang, J. Wang, and C. Chen, "Gold nanorods based platforms for light-mediated theranostics.," *Theranostics*, vol. 3, pp. 223–38, 2013.

[15] L. Vigderman, B. P. Khanal, and E. R. Zubarev, "Functional gold nanorods: synthesis, self-assembly, and sensing applications.," *Adv. Mater.*, vol. 24, pp. 4811–41, 5014, 2012.

[16] E. Chung, S. Y. Nam, L. M. Ricles, S. Y. Emelianov, and L. J. Suggs, "Evaluation of gold nanotracers to track adipose-derived stem cells in a PEGylated fibrin gel for dermal tissue engineering applications.," *Int. J. Nanomedicine*, vol. 8, pp. 325–36, 2013.

[17] J. Z. and K.-T. Y. and I. R. and R. H. and H. D. and L. Z. and M. T. S. and G. S. H. and Y. C. and P. N. Prasad, "Additive controlled synthesis of gold nanorods (GNRs) for two-photon luminescence imaging of cancer cells," *Nanotechnology*, vol. 21, no. 28, p. 285106, 2010.

[18] T. Wang, D. Halaney, D. Ho, M. D. Feldman, and T. E. Milner, "Two-photon luminescence properties of gold nanorods.," *Biomed. Opt. Express*, vol. 4, pp. 584–95, 2013.

[19] J. Vonnemann, N. Beziere, C. Böttcher, S. B. Riese, C. Kuehne, J. Dernedde, K. Licha, C. von Schacky, Y. Kosanke, M. Kimm, R. Meier, V. Ntziachristos, and R. Haag, "Polyglycerolsulfate functionalized gold nanorods as optoacoustic signal nanoamplifiers for in vivo bioimaging of rheumatoid arthritis.," *Theranostics*, vol. 4, pp. 629–41, 2014.

[20] J. M. Tucker-Schwartz, K. R. Beavers, W. W. Sit, A. T. Shah, C. L. Duvall, and M. C. Skala, "In vivo imaging of nanoparticle delivery and tumor microvasculature with multimodal optical coherence tomography," *Biomed. Opt. Express*, vol. 5, pp. 1731–1743, 2014.

[21] B. Wang, L. Kagemann, J. S. Schuman, H. Ishikawa, R. A. Bilonick, Y. Ling, I. A. Sigal, Z. Nadler, A. Francis, M. G. Sandrian, and G. Wollstein, "Gold Nanorods as a Contrast Agent for Doppler Optical Coherence Tomography," *PLoS One*, vol. 9, no. 3, p. e90690, Mar. 2014.

[22] S. Prabhulkar, J. Matthews, S. Rawal, and R. M. Awdeh, "Molecular Histopathology Using Gold Nanorods and Optical Coherence Tomography," *Investig. Ophthalmol. Vis. Sci.* , vol. 54 , no. 2 , pp. 1192–1200, Feb. 2013.

[23] C. A. Foss, G. L. Hornyak, J. A. Stockert, and C. R. Martin, "Template-Synthesized Nanoscopic Gold Particles: Optical Spectra and the Effects of Particle Size and Shape," *J. Phys. Chem.*, vol. 98, no. 11, pp. 2963–2971, Mar. 1994.

[24] N. R. Jana, L. Gearheart, and C. J. Murphy, "Seed-Mediated Growth Approach for Shape-Controlled Synthesis of Spheroidal and Rod-like Gold Nanoparticles Using a Surfactant Template," *Adv. Mater.*, vol. 13, no. 18, pp. 1389–1393, 2001.

[25] B. Nikoobakht and M. A. El-Sayed, "Preparation and Growth Mechanism of Gold Nanorods (NRs) Using Seed-Mediated Growth Method," *Chem. Mater.*, vol. 15, no. 10, pp. 1957–1962, Apr. 2003.

[26] S.-W. Tsai, J.-W. Liaw, Y.-C. Kao, M.-Y. Huang, C.-Y. Lee, L.-R. Rau, C.-Y. Huang, K.-C. Wei, and T.-C. Ye, "Internalized Gold Nanoparticles Do Not Affect the Osteogenesis and Apoptosis of MG63 Osteoblast-Like Cells: A Quantitative, In Vitro Study," *PLoS One*, vol. 8, no. 10, p. e76545, Oct. 2013.

[27] A. M. Alkilany, S. E. Lohse, and C. J. Murphy, "The gold standard: gold nanoparticle libraries to understand the nano-bio interface.," *Acc. Chem. Res.*, vol. 46, no. 3, pp. 650–61, Mar. 2013.

[28] Y. Pan, S. Neuss, A. Leifert, M. Fischler, F. Wen, U. Simon, G. Schmid, W. Brandau, and W. Jahnen-Dechent, "Size-dependent cytotoxicity of gold nanoparticles.," *Small*, vol. 3, no. 11, pp. 1941–9, Nov. 2007.

[29] S. Vijayakumar and S. Ganesan, "Size-dependent in vitro cytotoxicity assay of gold nanoparticles," *Toxicol. Environ. Chem.*, vol. 95, no. 2, pp. 277–287, Jan. 2013.

[30] S. Wang, W. Lu, O. Tovmachenko, U. S. Rai, H. Yu, and P. C. Ray, "Challenge in Understanding Size and Shape Dependent Toxicity of Gold Nanomaterials in Human Skin Keratinocytes.," *Chem. Phys. Lett.*, vol. 463, no. 1–3, pp. 145–149, Sep. 2008.

[31] L. Wang, X. Jiang, Y. Ji, R. Bai, Y. Zhao, X. Wu, and C. Chen, "Surface chemistry of gold nanorods: origin of cell membrane damage and cytotoxicity.," *Nanoscale*, vol. 5, no. 18, pp. 8384–91, Sep. 2013.

[32] A. Gole and C. J. Murphy, "Polyelectrolyte-Coated Gold Nanorods: Synthesis, Characterization and Immobilization," *Chem. Mater.*, vol. 17, no. 6, pp. 1325–1330, Mar. 2005.

[33] A. M. Alkilany, P. K. Nagaria, C. R. Hexel, T. J. Shaw, C. J. Murphy, and M. D. Wyatt, "Cellular uptake and cytotoxicity of gold nanorods: molecular origin of cytotoxicity and surface effects.," *Small*, vol. 5, no. 6, pp. 701–8, Mar. 2009.

[34] I. Gorelikov and N. Matsuura, "Single-step coating of mesoporous silica on cetyltrimethyl ammonium bromide-capped nanoparticles.," *Nano Lett.*, vol. 8, no. 1, pp. 369–73, Jan. 2008.

[35] A. S. Monem, N. Elbialy, and N. Mohamed, "Mesoporous silica coated gold nanorods loaded doxorubicin for combined chemo-photothermal therapy.," *Int. J. Pharm.*, vol. 470, no. 1–2, pp. 1–7, Aug. 2014.

[36] S. Shen, H. Tang, X. Zhang, J. Ren, Z. Pang, D. Wang, H. Gao, Y. Qian, X. Jiang, and W. Yang, "Targeting mesoporous silica-encapsulated gold nanorods for chemo-photothermal therapy with near-infrared radiation.," *Biomaterials*, vol. 34, no. 12, pp. 3150–8, Apr. 2013.

[37] Z. Zhang, L. Wang, J. Wang, X. Jiang, X. Li, Z. Hu, Y. Ji, X. Wu, and C. Chen, "Mesoporous silica-coated gold nanorods as a light-mediated multifunctional theranostic platform for cancer treatment.," *Adv. Mater.*, vol. 24, no. 11, pp. 1418–23, Mar. 2012.

[38] X. Wu, M. Wu, and J. X. Zhao, "Recent development of silica nanoparticles as delivery vectors for cancer imaging and therapy," *Nanomedicine Nanotechnology, Biol. Med.*, vol. 10, no. 2, pp. 297–312, Feb. 2014.

[39] X.-M. Zhu, C. Fang, H. Jia, Y. Huang, C. H. K. Cheng, C.-H. Ko, Z. Chen, J. Wang, and Y.-X. J. Wang, "Cellular uptake behaviour, photothermal therapy performance, and cytotoxicity of gold nanorods with various coatings.," *Nanoscale*, vol. 24, no. 17, pp. 1639–41, Aug. 2014.

[40] J. G. and E. A.-V. and K. H.-A. and M. S. and I. Chourpa, "Design strategies of hybrid metallic nanoparticles for theragnostic applications," *Nanotechnology*, vol. 24, no. 43, p. 432002, 2013.

[41] J. Choi, J. Yang, D. Bang, J. Park, J.-S. Suh, Y.-M. Huh, and S. Haam, "Targetable gold nanorods for epithelial cancer therapy guided by near-IR absorption imaging.," *Small*, vol. 8, no. 5, pp. 746–53, Mar. 2012.

[42] X. Qiu, Y. Wang, Y. Cui, Z. Sun, R. Liu, W. Huang, F. Zhao, Y. Zu, H. Yuan, X. Chang, and X. Gao, "Surface functionalized gold nanorods: tracking and observing live cell via three optical signals.," *J. Nanosci. Nanotechnol.*, vol. 12, no. 9, pp. 6893–9, Sep. 2012.

[43] T. Gong, D. Goh, M. Olivo, and K.-T. Yong, "In vitro toxicity and bioimaging studies of gold nanorods formulations coated with biofunctional thiol-PEG molecules and Pluronic block copolymers.," *Beilstein J. Nanotechnol.*, vol. 5, pp. 546–53, Jan. 2014.

[44] A. M. Alkilany and C. J. Murphy, "Gold nanoparticles with a polymerizable surfactant bilayer: synthesis, polymerization, and stability evaluation.," *Langmuir*, vol. 25, no. 24, pp. 13874–9, Dec. 2009.

[45] S. Bamrungsap, Z. Zhao, T. Chen, L. Wang, C. Li, T. Fu, and W. Tan, "Nanotechnology in therapeutics: a focus on nanoparticles as a drug delivery system.," *Nanomedicine (Lond).*, vol. 7, no. 8, pp. 1253–71, Aug. 2012.

[46] C. M. Dawidczyk, L. M. Russell, and P. C. Searson, "Nanomedicines for cancer therapy: state-of-the-art and limitations to pre-clinical studies that hinder future developments," *Front. Chem.*, vol. 2, Aug. 2014.

[47] L. Zhao, A. Seth, N. Wibowo, C.-X. Zhao, N. Mitter, C. Yu, and A. P. J. Middelberg, "Nanoparticle vaccines.," *Vaccine*, vol. 32, no. 3, pp. 327–37, Jan. 2014.

[48] Q.-L. Zhou, Z.-Y. Chen, Y.-X. Wang, F. Yang, Y. Lin, and Y.-Y. Liao, "Ultrasound-Mediated Local Drug and Gene Delivery Using Nanocarriers.," *Biomed Res. Int.*, vol. 2014, p. 963891, Jan. 2014.

[49] A. Kumar, X. Zhang, and X.-J. Liang, "Gold nanoparticles: emerging paradigm for targeted drug delivery system.," *Biotechnol. Adv.*, vol. 31, no. 5, pp. 593–606.

[50] E. H. Jeong, G. Jung, C. A. Hong, and H. Lee, "Gold nanoparticle (AuNP)-based drug delivery and molecular imaging for biomedical applications.," *Arch. Pharm. Res.*, vol. 37, no. 1, pp. 53–9, Jan. 2014.

[51] C. Yang, J. Uertz, D. Yohan, and B. D. Chithrani, "Peptide modified gold nanoparticles for improved cellular uptake, nuclear transport, and intracellular retention.," *Nanoscale*, Sep. 2014.

[52] D. Heinemann, S. Kalies, M. Schomaker, W. Ertmer, H. Murua Escobar, H. Meyer, and T. Ripken, "Delivery of proteins to mammalian cells via gold nanoparticle mediated laser transfection.," *Nanotechnology*, vol. 25, no. 24, p. 245101, Jun. 2014.

[53] S. Dhar, E. M. Reddy, A. Shiras, V. Pokharkar, and B. L. V. Prasad, "Natural Gum Reduced/Stabilized Gold Nanoparticles for Drug Delivery Formulations," *Chem. – A Eur. J.*, vol. 14, no. 33, pp. 10244–10250, Nov. 2008.

[54] D. Shi, C. Song, Q. Jiang, Z.-G. Wang, and B. Ding, "A facile and efficient method to modify gold nanorods with thiolated DNA at a low pH value," *Chem. Commun.*, vol. 49, no. 25, pp. 2533–2535, 2013.

[55] J. Wang, B. Dong, B. Chen, S. Xu, S. Zhang, W. Yu, C. Xu, and H. Song, "Glutathione modified gold nanorods with excellent biocompatibility and weak protein adsorption, targeting imaging and therapy toward tumor cells," *Dalt. Trans.*, vol. 42, no. 32, pp. 11548–11558, 2013.

[56] W. F. Zandberg, A. B. S. Bakhtiari, Z. Erno, D. Hsiao, B. D. Gates, T. Claydon, and N. R. Branda, "Photothermal release of small molecules from gold nanoparticles in live cells," *Nanomedicine Nanotechnology, Biol. Med.*, vol. 8, no. 6, pp. 908–915, Aug. 2012.

[57] L. Minati, V. Antonini, S. Torrengo, M. D. Serra, M. Boustta, X. Leclercq, C. Migliaresi, M. Vert, and G. Speranza, "Sustained in vitro release and cell uptake of doxorubicin adsorbed onto gold nanoparticles and covered by a polyelectrolyte complex layer," *Int. J. Pharm.*, vol. 438, no. 1–2, pp. 45–52, Nov. 2012.

[58] A. Elbakry, E.-C. Wurster, A. Zaky, R. Liebl, E. Schindler, P. Bauer-Kreisel, T. Blunk, R. Rachel, A. Goepferich, and M. Breunig, "Layer-by-Layer Coated Gold Nanoparticles: Size-Dependent Delivery of DNA into Cells," *Small*, vol. 8, no. 24, pp. 3847–3856, Dec. 2012.

[59] A. Elbakry, A. Zaky, R. Liebl, R. Rachel, A. Goepferich, and M. Breunig, "Layer-by-Layer Assembled Gold Nanoparticles for siRNA Delivery," *Nano Lett.*, vol. 9, no. 5, pp. 2059–2064, Mar. 2009.

[60] A. Wijaya, S. B. Schaffer, I. G. Pallares, and K. Hamad-Schifferli, "Selective release of multiple DNA oligonucleotides from gold nanorods.," *ACS Nano*, vol. 3, no. 1, pp. 80–6, Jan. 2009.

[61] K. V Chakravarthy, A. C. Bonoiu, W. G. Davis, P. Ranjan, H. Ding, R. Hu, J. B. Bowzard, E. J. Bergey, J. M. Katz, P. R. Knight, S. Sambhara, and P. N. Prasad, "Gold nanorod delivery of an ssRNA immune activator inhibits pandemic H1N1 influenza viral replication.," *Proc. Natl. Acad. Sci. U. S. A.*, vol. 107, no. 22, pp. 10172–7, Jun. 2010.

[62] H. Chen, X. Chi, B. Li, M. Zhang, Y. Ma, S. Achilefu, and Y. Gu, "Drug loaded multilayered gold nanorods for combined photothermal and chemotherapy," *Biomater. Sci.*, vol. 2, no. 7, pp. 996–1006, 2014.

[63] D. Saha and S. Bhattacharya, "Hydrocolloids as thickening and gelling agents in food: A critical review," *Journal of Food Science and Technology*, vol. 47. pp. 587–597, 2010.

[64] T. Osmałek, A. Froelich, and S. Tasarek, "Application of gellan gum in pharmacy and medicine," *International Journal of Pharmaceutics*, vol. 466. pp. 328–340, 2014.

[65] K. S. Kang, G. T. Veeder, P. J. Mirrasoul, T. Kaneko, and I. W. Cottrell, "Agar-like polysaccharide produced by a pseudomonas species: production and basic properties.," *Appl. Environ. Microbiol.*, vol. 43, pp. 1086–1091, 1982.

[66] P.-E. Jansson, B. Lindberg, and P. A. Sandford, "Structural studies of gellan gum, an extracellular polysaccharide elaborated by Pseudomonas elodea," *Carbohydrate Research*, vol. 124. pp. 135–139, 1983.

[67] M. Milas, X. Shi, and M. Rinaudo, "On the physicochemical properties of gellan gum.," *Biopolymers*, vol. 30, pp. 451–464, 1990.

[68] M. A. O'Neill, R. R. Selvendran, and V. J. Morris, "Structure of the acidic extracellular gelling polysaccharide produced by Pseudomonas elodea," *Carbohydrate Research*, vol. 124. pp. 123–133, 1983.

[69] R. Chandrasekaran, A. Radha, and V. G. Thailambal, "Roles of potassium ions, acetyl and L-glyceryl groups in native gellan double helix: An X-ray study," *Carbohydr. Res.*, vol. 224, pp. 1–17, 1992.

[70] M.-S. Kuo, A. J. Mort, and A. Dell, "Identification and location of l-glycerate, an unusual acyl substituent in gellan gum," *Carbohydr. Res.*, vol. 156, no. 0, pp. 173–187, Nov. 1986.

[71] R. Chandrasekaran, R. P. Millane, S. Arnott, and E. D. T. Atkins, "The crystal structure of gellan," *Carbohydr. Res.*, vol. 175, no. 1, pp. 1–15, Apr. 1988.

[72] T. Shimazaki, Y. Sato, K. Ogino, and E. Ogawa, "Influence of Ca2+-ion upon viscoelastic properties of gellan gum aqueous solutions," *Polym. Gels Networks*, vol. 3, no. 3, pp. 295–309, 1995.

[73] J. Tang, M. A. Tung, and Y. Zeng, "Gelling properties of gellan solutions containing monovalent and divalent cations," *J Food Sci*, vol. 62, p. 688–&, 1997.

[74] E. R. Morris, K. Nishinari, and M. Rinaudo, "Gelation of gellan – A review," *Food Hydrocoll.*, vol. 28, no. 2, pp. 373–411, Aug. 2012.

[75] C. S. F. Picone and R. L. Cunha, "Influence of pH on formation and properties of gellan gels," *Carbohydr. Polym.*, vol. 84, no. 1, pp. 662–668, Feb. 2011.

[76] L. Dai, X. Liu, and Z. Tong, "Critical behavior at sol–gel transition in gellan gum aqueous solutions with KCl and CaCl2 of different concentrations," *Carbohydr. Polym.*, vol. 81, no. 2, pp. 207–212, Jun. 2010.

[77] V. Evageliou, M. Mazioti, I. Mandala, and M. Komaitis, "Compression of gellan gels. Part II: Effect of sugars," *Food Hydrocoll.*, vol. 24, no. 4, pp. 392–397, Jun. 2010.

[78] H. Grasdalen and O. Smidsrød, "Gelation of gellan gum," *Carbohydrate Polymers*, vol. 7. pp. 371–393, 1987.

[79] J. T. Oliveira, T. C. Santos, L. Martins, M. A. Silva, A. P. Marques, A. G. Castro, N. M. Neves, and R. L. Reis, "Performance of new gellan gum hydrogels combined with human articular chondrocytes for cartilage regeneration when subcutaneously

implanted in nude mice.," *J. Tissue Eng. Regen. Med.*, vol. 3, no. 7, pp. 493–500, Oct. 2009.

[80] J. T. Oliveira, L. Martins, R. Picciochi, P. B. Malafaya, R. A. Sousa, N. M. Neves, J. F. Mano, and R. L. Reis, "Gellan gum: a new biomaterial for cartilage tissue engineering applications.," *J. Biomed. Mater. Res. A*, vol. 93, no. 3, pp. 852–63, Jun. 2010.

[81] J. T. Oliveira, L. S. Gardel, T. Rada, L. Martins, M. E. Gomes, and R. L. Reis, "Injectable gellan gum hydrogels with autologous cells for the treatment of rabbit articular cartilage defects.," *J. Orthop. Res.*, vol. 28, no. 9, pp. 1193–9, Sep. 2010.

[82] J. Silva-Correia, J. M. Oliveira, S. G. Caridade, J. T. Oliveira, R. A. Sousa, J. F. Mano, and R. L. Reis, "Gellan gum-based hydrogels for intervertebral disc tissue-engineering applications.," *J. Tissue Eng. Regen. Med.*, vol. 5, no. 6, pp. e97–107, Jun. 2011.

[83] S. J. Chang, Y.-T. Huang, S.-C. Yang, S.-M. Kuo, and M.-W. Lee, "In vitro properties of gellan gum sponge as the dental filling to maintain alveolar space," *Carbohydr. Polym.*, vol. 88, no. 2, pp. 684–689, Apr. 2012.

[84] R. Goyal, S. K. Tripathi, S. Tyagi, K. Ravi Ram, K. M. Ansari, Y. Shukla, D. Kar Chowdhuri, P. Kumar, and K. C. Gupta, "Gellan gum blended PEI nanocomposites as gene delivery agents: evidences from in vitro and in vivo studies.," *Eur. J. Pharm. Biopharm.*, vol. 79, no. 1, pp. 3–14, Sep. 2011.

[85] R. Goyal, S. K. Tripathi, S. Tyagi, K. R. Ram, K. M. Ansari, P. Kumar, Y. Shukla, D. K. Chowdhuri, and K. C. Gupta, "Gellan gum-PEI nanocomposites as efficient gene delivery agents.," *J. Biomed. Nanotechnol.*, vol. 7, no. 1, pp. 38–9, Feb. 2011.

[86] S. Dhar, V. Mali, S. Bodhankar, A. Shiras, B. L. V Prasad, and V. Pokharkar, "Biocompatible gellan gum-reduced gold nanoparticles: cellular uptake and subacute oral toxicity studies," *J. Appl. Toxicol.*, vol. 31, no. 5, pp. 411–420, Jul. 2011.

[87] S. Dhar, E. M. Reddy, A. Prabhune, V. Pokharkar, A. Shiras, and B. L. V Prasad, "Cytotoxicity of sophorolipid-gellan gum-gold nanoparticle conjugates and their doxorubicin loaded derivatives towards human glioma and human glioma stem cell lines," *Nanoscale*, vol. 3, no. 2, pp. 575–580, 2011.

[88] S. Dhar, P. Murawala, A. Shiras, V. Pokharkar, and B. L. V Prasad, "Gellan gum capped silver nanoparticle dispersions and hydrogels: cytotoxicity and in vitro diffusion studies," *Nanoscale*, vol. 4, no. 2, pp. 563–567, 2012.

[89] B. Sivakumar, R. G. Aswathy, R. Sreejith, Y. Nagaoka, S. Iwai, M. Suzuki, T. Fukuda, T. Hasumura, Y. Yoshida, T. Maekawa, and D. N. Sakthikumar, "Bacterial exopolysaccharide based magnetic nanoparticles: a versatile nanotool for cancer cell imaging, targeted drug delivery and synergistic effect of drug and hyperthermia mediated cancer therapy.," *J. Biomed. Nanotechnol.*, vol. 10, no. 6, pp. 885–99, Jun. 2014.

[90] C. Yi, D. Liu, C.-C. Fong, J. Zhang, and M. Yang, "Gold Nanoparticles Promote Osteogenic Differentiation of Mesenchymal Stem Cells through p38 MAPK Pathway," *ACS Nano*, vol. 4, no. 11, pp. 6439–6448, Oct. 2010.

[91] D. Zhang, D. Liu, J. Zhang, C. Fong, and M. Yang, "Gold nanoparticles stimulate differentiation and mineralization of primary osteoblasts through the ERK/MAPK signaling pathway," *Mater. Sci. Eng. C*, vol. 42, no. 0, pp. 70–77, Sep. 2014.

[92] D. Liu, J. Zhang, C. Yi, and M. Yang, "The effects of gold nanoparticles on the proliferation, differentiation, and mineralization function of MC3T3-E1 cells in vitro," *Chinese Sci. Bull.*, vol. 55, no. 11, pp. 1013–1019, Apr. 2010.

[93] J. M. Oliveira, R. A. Sousa, P. B. Malafaya, S. S. Silva, N. Kotobuki, M. Hirose, H. Ohgushi, J. F. Mano, and R. L. Reis, "In vivo study of dendronlike nanoparticles for stem cells 'tune-up': from nano to tissues," *Nanomedicine Nanotechnology, Biol. Med.*, vol. 7, no. 6, pp. 914–924, Dec. 2011.

[94] N. Monteiro, A. Martins, D. Ribeiro, S. Faria, N. A. Fonseca, J. N. Moreira, R. L. Reis, and N. M. Neves, "On the use of dexamethasone-loaded liposomes to induce the osteogenic differentiation of human mesenchymal stem cells," *J. Tissue Eng. Regen. Med.*, p. n/a–n/a, Sep. 2013.

[95] C. J. Orendorff and C. J. Murphy, "Quantitation of Metal Content in the Silver-Assisted Growth of Gold Nanorods," *J. Phys. Chem. B*, vol. 110, no. 9, pp. 3990–3994, Feb. 2006.

[96] A. J. Salgado, J. E. Figueiredo, O. P. Coutinho, and R. L. Reis, "Biological response to pre-mineralized starch based scaffolds for bone tissue engineering.," *J. Mater. Sci. Mater. Med.*, vol. 16, no. 3, pp. 267–75, Mar. 2005.

[97] J. Zhu, K.-T. Yong, I. Roy, R. Hu, H. Ding, L. Zhao, M. T. Swihart, G. S. He, Y. Cui, and P. N. Prasad, "Additive controlled synthesis of gold nanorods (GNRs) for two-photon luminescence imaging of cancer cells.," *Nanotechnology*, vol. 21, no. 28, p. 285106, Jul. 2010.

[98] J. C. Y. Kah, A. Zubieta, R. A. Saavedra, and K. Hamad-Schifferli, "Stability of gold nanorods passivated with amphiphilic ligands.," *Langmuir*, vol. 28, no. 24, pp. 8834–44, Jun. 2012.

[99] M. Sethi, G. Joung, and M. R. Knecht, "Stability and electrostatic assembly of au nanorods for use in biological assays.," *Langmuir*, vol. 25, no. 1, pp. 317–25, Jan. 2009.

[100] F. Yang, S. Xia, C. Tan, and X. Zhang, "Preparation and evaluation of chitosan-calcium-gellan gum beads for controlled release of protein," *Eur. Food Res. Technol.*, vol. 237, no. 4, pp. 467–479, May 2013.

[101] C. Pautke, M. Schieker, T. Tischer, A. Kolk, P. Neth, W. Mutschler, and S. Milz, "Characterization of osteosarcoma cell lines MG-63, Saos-2 and U-2 OS in comparison to human osteoblasts.," *Anticancer Res.*, vol. 24, no. 6, pp. 3743–8.

[102] E. Arrigoni, S. Lopa, L. de Girolamo, D. Stanco, and A. T. Brini, "Isolation, characterization and osteogenic differentiation of adipose-derived stem cells: from small to large animal models.," *Cell Tissue Res.*, vol. 338, no. 3, pp. 401–11, Dec. 2009.

[103] T. M. Buttke, J. A. McCubrey, and T. C. Owen, "Use of an aqueous soluble tetrazolium/formazan assay to measure viability and proliferation of lymphokine-dependent cell lines," *J. Immunol. Methods*, vol. 157, no. 1–2, pp. 233–240, Jan. 1993.

[104] K. Shapero, F. Fenaroli, I. Lynch, D. C. Cottell, A. Salvati, and K. A. Dawson, "Time and space resolved uptake study of silica nanoparticles by human cells.," *Mol. Biosyst.*, vol. 7, no. 2, pp. 371–8, Feb. 2011.

[105] B. Rituper, A. Guček, J. Jorgačevski, A. Flašker, M. Kreft, and R. Zorec, "High-resolution membrane capacitance measurements for the study of exocytosis and endocytosis," *Nat. Protoc.*, vol. 8, no. 6, pp. 1169–1183, Jun. 2013.

[106] J. S. Park, K. Na, D. G. Woo, H. N. Yang, and K.-H. Park, "Determination of dual delivery for stem cell differentiation using dexamethasone and TGF-beta3 in/on polymeric microspheres.," *Biomaterials*, vol. 30, no. 27, pp. 4796–805, Sep. 2009.

[107] Y. Moussy, L. Hersh, and P. Dungel, "Distribution of [3H]dexamethasone in rat subcutaneous tissue after delivery from osmotic pumps.," *Biotechnol. Prog.*, vol. 22, no. 3, pp. 819–24.

[108] J. F. Mano, G. A. Silva, H. S. Azevedo, P. B. Malafaya, R. A. Sousa, S. S. Silva, L. F. Boesel, J. M. Oliveira, T. C. Santos, A. P. Marques, N. M. Neves, and R. L. Reis, "Natural origin biodegradable systems in tissue engineering and regenerative medicine: present status and some moving trends.," *J. R. Soc. Interface*, vol. 4, pp. 999–1030, 2007.

- *This page was intentionally left blank.* -